

Scalable Marginal Likelihood Estimation for Model Selection in Deep Learning

Alexander Immer^{1,2} Matthias Bauer^{†3,4} Vincent Fortuin¹ Gunnar Rätsch^{1,2} Mohammad Emtiyaz Khan⁵

Abstract

Marginal-likelihood based model-selection, even though promising, is rarely used in deep learning due to estimation difficulties. Instead, most approaches rely on validation data, which may not be readily available. In this work, we present a scalable marginal-likelihood estimation method to select both hyperparameters and network architectures, based on the training data alone. Some hyperparameters can be estimated online during training, simplifying the procedure. Our marginal-likelihood estimate is based on Laplace’s method and Gauss-Newton approximations to the Hessian, and it outperforms cross-validation and manual-tuning on standard regression and image classification datasets, especially in terms of calibration and out-of-distribution detection. Our work shows that marginal likelihoods can improve generalization and be useful when validation data is unavailable (e.g., in nonstationary settings).

1. Introduction

Bayesian deep learning has made great strides on approximate inference but little has been done regarding model selection. Bayesian predictive distributions have been used to improve calibration, detect out-of-distribution data, and sometimes even improve the accuracy (Osawa et al., 2019; Maddox et al., 2019). To that end, a wide variety of scalable approximate inference methods have been explored, including Laplace’s method (Ritter et al., 2018), variational approximations (Blundell et al., 2015; Khan et al., 2018), sampling methods (Wenzel et al., 2020), and ensembles (Lakshminarayanan et al., 2017). Still, there is not much work on model-selection, even though it was one of the original motivations for Bayesian neural networks (Buntine & Weigend, 1991; MacKay, 1995; Neal, 1995).

¹Department of Computer Science, ETH Zurich, Switzerland
²Max Planck ETH Center for Learning Systems (CLS) ³Max Planck Institute for Intelligent Systems, Germany ⁴University of Cambridge, UK ⁵RIKEN Center for Advanced Intelligence Project, Japan, [†]M.B. is now at DeepMind, UK. Correspondence to: Alexander Immer <alexander.immer@inf.ethz.ch>. *Proceedings of the 38th International Conference on Machine Learning*, PMLR 139, 2021. Copyright 2021 by the author(s).

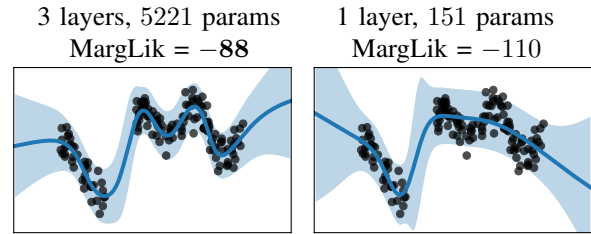


Figure 1: A deeper 3-layer network (*left*) has a better marginal likelihood compared to a 1-layer network (*right*). This agrees with the fit where the deeper network appears to explain the ‘sinusoidal’ trend better. We optimize the prior and noise variance on marginal likelihood estimates *during training* (see Alg. 1 and Sec. 4.1 for details).

Bayesian model-selection uses the *marginal likelihood*—the normalizing constant of the posterior distribution—which can be estimated solely from training data and without any validation data. Also known as *empirical Bayes* (Robbins, 1955) or *type-II maximum likelihood* learning (Rasmussen & Williams, 2006), it is closely related to Occam’s razor (Jefferys & Berger, 1992; Rasmussen & Ghahramani, 2001; MacKay, 2003). It can also be seen as a form of cross-validation based on the training data (Fong & Holmes, 2020), and it is commonly used in Gaussian processes (GPs) and Deep GPs to select hyperparameters (Rasmussen & Williams, 2006; Damianou & Lawrence, 2013) or even learn invariances from data (van der Wilk et al., 2018; Dutordoir et al., 2020). However, it is rarely used in deep learning because it is challenging to estimate (Llorente et al., 2020).

The marginal likelihood is intractable for even medium-sized neural-network models, and most Bayesian deep learning approaches simply use validation data (Khan et al., 2018; Zhang et al., 2018; Osawa et al., 2019). Originally, MacKay (1995) advocated the use of Laplace’s method for small-scale neural networks. This requires Hessian computations and does not scale to large problems. Recently, Khan et al. (2019) showed promising results for small-scale regression using a GP viewpoint of deep networks, and Lyle et al. (2020) used infinite-width neural networks (also GPs).

The goal of this paper is to provide a scalable and online version of MacKay’s original proposal, and apply it to modern, larger models used in deep learning. We propose a scalable Laplace’s method to approximate the marginal like-

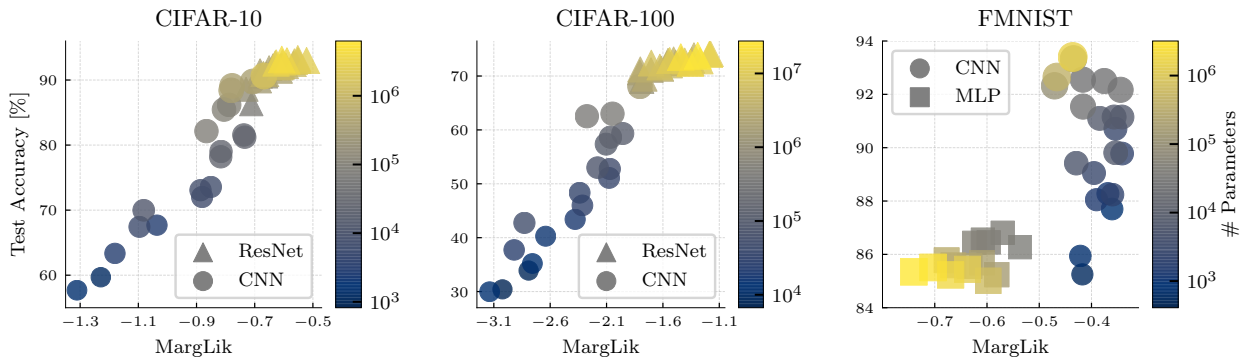


Figure 2: Each dot above shows a model of different size and/or architecture (around 40 models per plot of varying widths and depths). Models with higher training marginal-likelihood tend to have higher test accuracy. For similar performance, smaller models tend to have a higher marginal-likelihood as desired. Marker size and color changes with the number of parameters. See Sec. 4.3 for details and App. C.5 for a full list of models with accuracy and marginal-likelihood estimates.

likelihood and select both the hyperparameters and network architectures. Differentiable hyperparameters can be optimized *during* training in an online fashion (unlike MacKay (1995)’s original proposal and Khan et al. (2019)’s recent approach), and discrete ones can be selected after training.

The method relies on the Generalized Gauss-Newton (GGN) and the Empirical Fisher (EF) approximation to the Hessian. The full GGN and EF can also be extremely expensive and we reduce the cost by using additional diagonal and block-diagonal approximations (Martens & Grosse, 2015; Botev et al., 2017). All these approximations have been used in approximate inference before (Khan et al., 2018; Zhang et al., 2018; Ritter et al., 2018; Osawa et al., 2019; Foresee & Hagan, 1997; Khan et al., 2019), but they have not been applied to model selection and their effectiveness for marginal likelihood estimation has also been unknown. Unlike our proposal, the method by Khan et al. (2019) is limited to regression and uses the full but intractable GGN approximation. Blundell et al. (2015) also used the variational lower-bound for hyperparameter optimization but found it to give worse results.

Our main contribution is to show that, even after making these approximations to improve scalability, the estimated marginal likelihoods can faithfully select reasonable models (see Figs. 1 and 2). Our method achieves performance on par or better than cross-validation on a range of regression and classification benchmarks. The best architecture identified by the marginal likelihood aligns with the test performance (see Fig. 2). It aligns well with the empirical observation that ResNets often perform better than the standard convolutional networks, which in turn are observed to give better results than their fully-connected counterparts. Overall, our work supports the long-held hypothesis that the marginal likelihood is effective for model selection in deep learning, and shows that a relatively cheap and simple approximation can achieve competitive results.

2. Background

In this paper, we consider supervised learning tasks with inputs $\mathbf{x}_n \in \mathbb{R}^D$ and C -dimensional vector outputs \mathbf{y}_n (real or categorical outcomes), and denote the data as the set $\mathcal{D} = \{(\mathbf{x}_n, \mathbf{y}_n)\}_{n=1}^N$ of N training-example pairs.

Bayesian models. We denote by $\mathbf{f}(\mathbf{x}, \boldsymbol{\theta})$ the C -dimensional real-valued output of a neural network with parameters $\boldsymbol{\theta} \in \mathbb{R}^P$, specified by a model \mathcal{M} which typically consists of a network architecture and *hyperparameters*. A Bayesian model can then be defined using a likelihood and a prior, to get the posterior distribution: $p(\boldsymbol{\theta}|\mathcal{D}, \mathcal{M}) \propto p(\mathcal{D}|\boldsymbol{\theta}, \mathcal{M})p(\boldsymbol{\theta}|\mathcal{M})$. We assume that the data examples are sampled *i.i.d.* from $p(\mathbf{y}|\mathbf{f}(\mathbf{x}, \boldsymbol{\theta}), \mathcal{M})$. The normalizing constant of the posterior, also known as the *marginal likelihood*, is given by the following expression:

$$p(\mathcal{D}|\mathcal{M}) = \int \prod_{n=1}^N p(\mathbf{y}_n|\mathbf{f}(\mathbf{x}_n, \boldsymbol{\theta}), \mathcal{M})p(\boldsymbol{\theta}|\mathcal{M}) d\boldsymbol{\theta}. \quad (1)$$

The model \mathcal{M} might consist of the choice of network-architecture (CNN, ResNet, etc.) and hyperparameters of the likelihood and prior, for example, observation noise and prior variances. Some of these are continuous parameters while others are discrete. Our goal is to use the marginal likelihood to select such parameters.

Bayesian model comparison. The marginal likelihood in Eq. 1 can be seen as a probability distribution over the space of all datasets (of size N) given the model \mathcal{M} . The distribution is expected to be wider for complex models, because such models can generate data of more variety than simpler models. Given the training data \mathcal{D} , a model too simple or too complex will therefore be assigned a lower probability $p(\mathcal{D}|\mathcal{M})$, naturally yielding *Occam’s razor* (Blumer et al., 1987; Jefferys & Berger, 1992; Rasmussen & Ghahramani, 2001). See Fig. 3.13 in Bishop (2006) for an illustration. A simple method is to pick the model that assigns the highest

probability to the training data,

$$\mathcal{M}_* = \arg \max_{\mathcal{M}} p(\mathcal{D}|\mathcal{M}). \quad (2)$$

This procedure is also called *type-II maximum likelihood estimation* or *empirical Bayes* (MacKay, 2003); it is commonly used in the Gaussian process literature to find the hyperparameters of the kernel process function (Rasmussen & Williams, 2006). Additionally, we can reapply Bayes rule with the marginal likelihood as the *likelihood* and an additional prior distribution $p(\mathcal{M})$ over the models (MacKay, 1992; 2003). Eq. 2 can then be seen as a special case of a *maximum a-posteriori* (MAP) estimate with a uniform prior.

Laplace’s method. Using the marginal likelihood for neural-network model selection was originally proposed by MacKay (1992), who used Laplace’s method to approximate Eq. 1. The method relies on a local quadratic approximation of $\log p(\theta|\mathcal{D}, \mathcal{M})$, around a maximum θ_* , resulting in a Gaussian approximation to $p(\theta|\mathcal{D}, \mathcal{M})$, denoted by $q(\theta|\mathcal{D}, \mathcal{M})$, and an approximation to the marginal likelihood, denoted by $q(\mathcal{D}|\mathcal{M})$ and shown below,

$$\begin{aligned} \log p(\mathcal{D}|\mathcal{M}) &\approx \log q(\mathcal{D}|\mathcal{M}) \\ &:= \log p(\mathcal{D}, \theta_*|\mathcal{M}) - \frac{1}{2} \log \left| \frac{1}{2\pi} \mathbf{H}_{\theta_*} \right|, \end{aligned} \quad (3)$$

with Hessian $\mathbf{H}_{\theta} := -\nabla_{\theta\theta}^2 \log p(\mathcal{D}, \theta|\mathcal{M})$. However, computing \mathbf{H}_{θ} , a large matrix of size $P \times P$, and its determinant is infeasible in general. We refer to the log marginal likelihood as *marginLik* and report its value normalized by the number of training examples.

Using the above objective to select models can also lead to better generalization. The log-determinant in Eq. 3 favors Hessians with small eigenvalues and is thus closely related to low curvature and flatness of a solution’s neighborhood. Such *flat minima* have been argued to generalize better than sharper ones (Hochreiter & Schmidhuber, 1997), a claim that is supported empirically (Keskar et al., 2016; Jiang et al., 2019; Maddox et al., 2019) and has also been formalized using PAC-Bayesian generalization bounds (Dziugaite & Roy, 2017). We can therefore expect models selected using the marginal-likelihood to have similar properties. The local Gaussian approximation above may not always be sufficient, and the goal of this paper is to investigate its capacity to measure complexity of large neural networks.

Hessian approximations. Recently, scalable approximations to the Hessian \mathbf{H}_{θ} , such as those based on the generalized Gauss-Newton (GGN) and empirical Fisher (EF), have been applied to approximate Bayesian inference (Khan et al., 2018; Zhang et al., 2018; Ritter et al., 2018; Osawa et al., 2019; Immer et al., 2021; Kristiadi et al., 2020), but their application to marginal-likelihood estimation or model selection has not yet been explored, except by Khan et al. (2019) on small regression tasks with a full GGN.

The GGN approximation to the log-joint Hessian is based on the *Jacobian* matrix $\mathbf{J}_{\theta}(\mathbf{x}) \in \mathbb{R}^{C \times P}$ of the network features with entries $[\mathbf{J}_{\theta}(\mathbf{x})]_{ci} = \frac{\partial f_c(\mathbf{x}, \theta)}{\partial \theta_i}$, as well as the Hessians of the log-likelihood and the log-prior,

$\Lambda(\mathbf{y}; \mathbf{f}) := -\nabla_{\mathbf{ff}}^2 \log p(\mathbf{y}|\mathbf{f})$, $\mathbf{P}_{\theta} := -\nabla_{\theta\theta}^2 \log p(\theta|\mathcal{M})$, respectively. The GGN approximation is then given by

$$\mathbf{H}_{\theta} \approx \mathbf{H}_{\theta}^{\text{GGN}} = \mathbf{J}_{\theta}^T \mathbf{L}_{\theta} \mathbf{J}_{\theta} + \mathbf{P}_{\theta}, \quad (4)$$

where \mathbf{J}_{θ} is an $NC \times P$ matrix formed by *stacking* N Jacobians $\mathbf{J}_{\theta}(\mathbf{x}_n)$ overall \mathbf{x}_n in \mathcal{D} , and \mathbf{L}_{θ} is a $NC \times NC$ block-diagonal matrix with blocks $\Lambda(\mathbf{y}_n; \mathbf{f}(\mathbf{x}_n, \theta))$.

The expression for the GGN approximation in Eq. 4 is equivalent to the Fisher information matrix (Kunstner et al., 2019); we therefore also consider the *empirical Fisher* (EF) approximation to the Hessian, which relies on an outer product of the gradients $\mathbf{G}_{\theta}(\mathbf{x}) = \nabla_{\theta} \log p(\mathbf{y}|\mathbf{f}(\mathbf{x}, \theta), \mathcal{M}) \in \mathbb{R}^P$:

$$\mathbf{H}_{\theta} \approx \mathbf{H}_{\theta}^{\text{EF}} = \mathbf{G}_{\theta}^T \mathbf{G}_{\theta} + \mathbf{P}_{\theta}, \quad (5)$$

where \mathbf{G}_{θ} is an $N \times P$ matrix of stacked gradients $\mathbf{G}_{\theta}(\mathbf{x}_n)$ for all $\mathbf{x}_n \in \mathcal{D}$. The complexities of the GGN and EF are $\mathcal{O}(P^2 NC + PNC^2)$ and $\mathcal{O}(P^2 N)$, respectively. The EF is therefore $\mathcal{O}(C)$ cheaper to compute as C is typically much smaller than P . For details, see App. B. Throughout, we use "Laplace-GGN" and "Laplace-EF" to refer to Laplace’s method where the Hessian has been approximated by using the GGN or EF, respectively.

3. Model Selection with Laplace-GGN and -EF

We propose to use GGN and EF approximations for scalable marginal-likelihood estimation based on Laplace’s method. Our method involves two key steps:

Step 1. During training, we update differentiable hyperparameters of \mathcal{M} by using gradients of Eq. 3. See line 8 in Alg. 1 and cf. Fig. 3 (left) for an example.

Step 2. After training, we use the marginal likelihood of the trained model to make discrete choices, e.g., to select the network architecture as shown in Fig. 1, or to choose between several trained models, shown in Fig. 3 (right).

We first describe each of these steps and then give details about efficient Hessian-determinant computations.

3.1. Step 1: Online model selection during training

Here we alternate between optimizing the network parameters θ and updating the continuous hyperparameters $\mathcal{M}^{\theta} \subseteq \mathcal{M}$ that appear in the marginal likelihood in a differentiable way. Such differentiable hyperparameters may include the observation noise of the likelihood, the variances of the Gaussian prior, or the softmax temperature parameter. The resulting algorithm is outlined in Alg. 1.

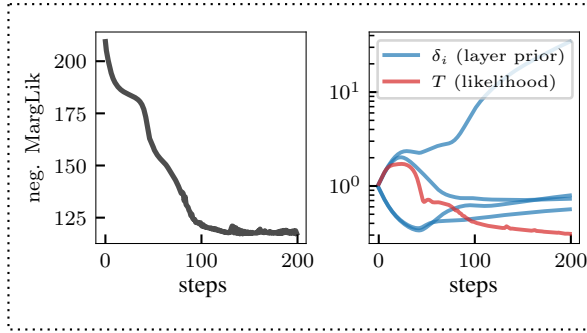
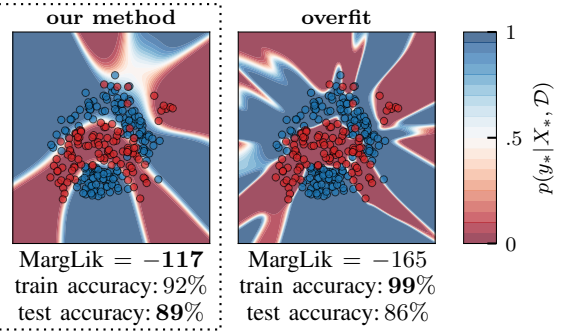
Step 1: Optimize Marginal-Likelihood wrt. hyperparameters

Step 2: Compare marginal likelihood of models


Figure 3: Proposed method for model selection using the marginal likelihood. In Step 1, we apply our online algorithm (Alg. 1) to optimize the marginal likelihood estimate (Eq. 3) with respect to the differentiable hyperparameters (*here*: prior precision δ_i per layer and softmax temperature T). In Step 2, we compare the resulting model (*left*) to an overfitting model (*right*) with higher training accuracy but lower test accuracy; both models have the same architecture. The Laplace-GGN marginal likelihood estimate $\log q(\mathcal{D}|\mathcal{M})$ correctly identifies the model that generalizes better. See Sec. 4.1 for details.

To optimize the network parameters θ we perform regular neural network training on the *maximum a posteriori* (MAP) objective in Eq. 6 using stochastic optimizers like ADAM (Kingma & Ba, 2015) or SGD (cf. line 4 in Alg. 1),

$$\log p(\mathcal{D}, \theta|\mathcal{M}) = \sum_{n=1}^N \log p(\mathbf{y}_n|\mathbf{x}_n, \theta) + \log p(\theta). \quad (6)$$

To optimize the continuous hyperparameters \mathcal{M}^θ , we perform gradient ascent on the marginal likelihood estimate (Eq. 3). Because of computational considerations further detailed in Sec. 3.4, we only do so every F epochs after an initial burn-in period of B epochs and then perform K update steps with step size $\gamma > 0$ (cf. lines 6-10 in Alg. 1):

$$\mathcal{M}^\theta \leftarrow \mathcal{M}^\theta + \gamma \nabla_{\mathcal{M}^\theta} \log q(\mathcal{D}|\mathcal{M}). \quad (7)$$

The marginal likelihood estimate can be updated cheaply for each of the K iterations (cf. App. B). Fig. 3 (*left*) illustrates this optimization of the Gaussian prior-variances for each layer as well as the softmax temperature of the likelihood. We can also use the marginal-likelihood for early stopping *without* validation data.

Note that the parameters θ_* in Eq. 3 are assumed to be the MAP estimate, however this is not true during training at some θ . We also try another method derived from a local integration in App. A.1 instead, but empirically this does not yield good results and is more expensive. We discuss the choice of hyperparameters of Alg. 1 in Sec. 3.4.

3.2. Step 2: Model selection after training

To choose between two discrete model alternatives, such as different architectures, we compare their marginal likelihood estimates after training. This step is a basic hypothesis test, where we compare two models \mathcal{M} and \mathcal{M}' and choose

Algorithm 1 Marginal likelihood based training

- 1: **Input:** dataset \mathcal{D} , likelihood $p(\mathcal{D}|\theta, \mathcal{M})$, prior $p(\theta|\mathcal{M})$. Initial model \mathcal{M} , step size γ , steps K , burn-in epochs B , marglik frequency F . GGN or EF.
 - 2: initialize θ of the neural network
 - 3: **for each epoch do**
 - 4: $\theta \leftarrow \text{trainEpoch}(\text{objective in Eq. 6})$
 - 5: **if** $\text{epoch} > B$ and $\text{epoch} \bmod F = 0$ **then**
 - 6: compute $\log q(\mathcal{D}|\mathcal{M})$ (Eq. 3) with $\mathbf{H}_\theta^{\text{GGN}}$ or $\mathbf{H}_\theta^{\text{EF}}$
 - 7: **for** K steps **do**
 - 8: $\mathcal{M}^\theta \leftarrow \mathcal{M}^\theta + \gamma \nabla_{\mathcal{M}^\theta} \log q(\mathcal{D}|\mathcal{M})$
 - 9: update \mathcal{M} and $\log q(\mathcal{D}|\mathcal{M})$
 - 10: **end for**
 - 11: **end if**
 - 12: **end for**
 - 13: Return marginal likelihood $\log q(\mathcal{D}|\mathcal{M})$ and optionally posterior approximation $q(\theta|\mathcal{D}, \mathcal{M})$.
-

the more likely model given the data according to the likelihood ratio $p(\mathcal{D}|\mathcal{M})/p(\mathcal{D}|\mathcal{M}')$, which is the most powerful statistical test for this purpose (Neyman & Pearson, 1933). In terms of the marginal likelihood, we only need to choose the model with a higher value (cf. Fig. 1 and Fig. 3 (*right*)).

3.3. Scalable Laplace approximations

Efficient determinant computation. Scalable marginal likelihood estimation (Eq. 3) relies on an efficient computation of the determinant of the GGN or EF approximation of the Hessian (Eqs. 4 and 5). When N is small, we can use the Woodbury matrix identity to rewrite the determinant of the Hessian (a $P \times P$ matrix) in terms of determinants of matrices whose size only depends on the number of data

points N and outputs (e.g., classes) C instead:

$$\begin{aligned} |\mathbf{H}_\theta^{\text{GGN}}| &= \left| \underbrace{\mathbf{J}_\theta^\top \mathbf{L}_\theta \mathbf{J}_\theta + \mathbf{P}_\theta}_{P \times P} \right| = \left| \underbrace{\mathbf{J}_\theta \mathbf{P}_\theta^{-1} \mathbf{J}_\theta^\top + \mathbf{L}_\theta^{-1}}_{NC \times NC} \right| |\mathbf{L}_\theta| |\mathbf{P}_\theta| \\ |\mathbf{H}_\theta^{\text{EF}}| &= \left| \underbrace{\mathbf{G}_\theta^\top \mathbf{G}_\theta + \mathbf{P}_\theta}_{P \times P} \right| = \left| \underbrace{\mathbf{G}_\theta \mathbf{P}_\theta^{-1} \mathbf{G}_\theta^\top + \mathbf{I}_N}_{N \times N} \right| |\mathbf{P}_\theta|. \end{aligned} \quad (8)$$

The determinants $|\mathbf{P}_\theta|$ (though still $P \times P$) and $|\mathbf{L}_\theta|$ are usually cheap to compute as the prior $p(\theta)$ often factorizes across parameters and \mathbf{L}_θ is block-diagonal. When neither $\mathcal{O}(N^3)$ nor $\mathcal{O}(P^3)$ are tractable, we consider the following structured GGN approximations of different sparsities.

Kronecker-factored Laplace. The Kronecker-factored (KFAC) GGN approximation is based on a block-diagonal approximation to $\mathbf{H}_\theta^{\text{GGN}}$ and is specified by a Kronecker product per layer (Martens & Grosse, 2015; Botev et al., 2017). The GGN of the l -th layer of the neural network is approximated as $[\mathbf{J}_\theta^\top \mathbf{L}_\theta \mathbf{J}_\theta]_l \approx \mathbf{Q}_l \otimes \mathbf{W}_l$ where \mathbf{Q}_l is computed from the gradient by backpropagation and \mathbf{W}_l depends on the input to the l -th layer. \mathbf{W}_l and \mathbf{Q}_l are quadratic in the l -th layer’s input and output size, respectively. Let $\mathbf{q}^{(l)} \in \mathbb{R}^{D_l}$ and $\mathbf{w}^{(l)} \in \mathbb{R}^{D_l}$ be the eigenvalues of \mathbf{Q}_l and \mathbf{W}_l , respectively. If the prior Hessian \mathbf{P}_θ is isotropic per layer, that is, the l -th block-diagonal entry of \mathbf{P}_θ is given by $p_\theta^{(l)} \mathbf{I}_l$, then we can compute the determinant for the Laplace-GGN efficiently as

$$|\mathbf{H}_\theta^{\text{GGN}}| \approx |\mathbf{H}_\theta^{\text{KFAC}}| = \prod_l \prod_{ij} \mathbf{q}_i^{(l)} \mathbf{w}_j^{(l)} + p_\theta^{(l)}. \quad (9)$$

In contrast to the typical use of Kronecker-factored approximations in optimization (Martens & Grosse, 2015; Botev et al., 2017) and approximate inference (Ritter et al., 2018; Zhang et al., 2018), we do not use damping which would distort the Laplace-GGN (cf. App. A.3 for discussion and ablation experiment). Computationally, the Kronecker-factored Laplace-GGN is cheaper than the full Laplace-GGN because we only need to decompose matrices that are quadratic in the number of neurons per layer. This number typically does not exceed a few thousand.

Diagonal Laplace. The diagonal Laplace approximates the GGN or EF by their diagonal, which allows for the cheap computation of the determinants

$$|\mathbf{H}_\theta^{\text{GGN}}| \approx \prod_p [\mathbf{H}_\theta^{\text{GGN}}]_{pp} \text{ and } |\mathbf{H}_\theta^{\text{EF}}| \approx \prod_p [\mathbf{H}_\theta^{\text{EF}}]_{pp}. \quad (10)$$

Here, $[\mathbf{H}]_{pp}$ denotes the diagonal entries of \mathbf{H} . The computation of the diagonal GGN still scales with the number of outputs C due to the dependence on the block-diagonal \mathbf{L}_θ . In contrast, the diagonal EF is very cheap to compute because it only requires the sum of point-wise squared individual gradients over the training data. Despite their simplicity and the hypothesis by MacKay (1992) that they are “no good”, we find that these approximations work well in practice. Especially for convolutional neural networks,

the diagonal approximations provide a cost-effective alternative to block-diagonal approximations when used in Alg. 1. This is in contrast to the predictive performance of diagonal Laplace approximations, which are often significantly worse than their less sparse counterparts (Ritter et al., 2018; Immer et al., 2021).

3.4. Computational considerations

The overall runtime of our algorithm depends on the frequency F with which we estimate the marginal likelihood, the number of consecutive hyperparameter update steps K , as well as the burn-in period B . Furthermore, the cost of each marginal likelihood estimation (line 6 in Alg. 1) and marginal likelihood update (line 9 in Alg. 1) depends on the specific approximation of the Hessian used. Here, we discuss the most important aspects briefly. See App. B for more details and discussion, including computation and memory complexities.

Estimation of the marginal likelihood (Eq. 3) requires one full pass over the training data: While its first term, the log joint $p(\mathcal{D}, \theta | \mathcal{M})$ (Eq. 6), decomposes into individual terms per data point and can, therefore, be estimated on minibatches, this is not the case for the log determinant of the Hessian. However, this initial estimation cost amortizes over the K consecutive update steps for the hyperparameters (Alg. 1 lines 7 to 10), as the most expensive computations can be reused. Therefore, it makes sense to perform many update steps (K large) but do so at a lower frequency (estimation frequency F low). We typically use $K = 100$ update steps in large-scale experiments and perform marginal likelihood estimation every $F = 1$ epochs for small-scale experiments or $F = 5$ to 10 epochs for larger experiments. In contrast to MacKay (1995), these updates are continuous during training, instead of a single update and re-training which would be prohibitive.

We use ADAM for the gradient updates of the hyperparameters in Eq. 7 and line 8 of Alg. 1. We can use a slightly higher learning rate than default (γ between 0.01 and 1) without divergence because the gradients are not stochastic (Bottou, 2010). Similar to the approach by Lyle et al. (2020), our marginal likelihood estimate can be used for early stopping or to save models so that we end up using the model that achieved the best marginal likelihood during training in Alg. 1. Overall, we find that the online algorithm is robust to different settings of K , F , B , and γ , and it is not difficult to monitor convergence of the marginal likelihood and hyperparameters, of which there are fewer than model parameters. In our experiments, we reliably optimize up to around 400 hyperparameters in the case of a ResNet. Typically, our algorithm does not need more epochs to converge than standard training. For further discussion of the robustness to hyperparameters, see App. C.6.

4. Experiments

We compare our method to model selection by cross-validation and also to manually selected models. Depending on the problem size, we use different variants of the Laplace-GGN approximation. On smaller scale UCI (Dua & Graff, 2017) and toy examples, we use the full GGN and EF determinants and the Kronecker-factored approximation. On larger problems, we use the Kronecker-factored and the diagonal Laplace-GGN and EF approximations.

We also compare the posterior predictive obtained by a Laplace-GGN posterior approximation (Ritter et al., 2018; Immer et al., 2021), defined in Eq. 11, to the MAP prediction, defined in Eq. 12,

$$p_{\text{dist}}(\mathbf{y}^* | \mathbf{x}^*, \mathcal{D}) = \frac{1}{S} \sum_s p(\mathbf{y}^* | \mathbf{f}_{\text{lin}}^{\theta_s}(\mathbf{x}^*, \boldsymbol{\theta}_s), \mathcal{M}_*), \quad (11)$$

$$p_{\text{MAP}}(\mathbf{y}^* | \mathbf{x}^*, \mathcal{D}) = p(\mathbf{y}^* | \mathbf{f}(\mathbf{x}^*, \boldsymbol{\theta}_*), \mathcal{M}_*). \quad (12)$$

Here, $\mathbf{f}_{\text{lin}}^{\theta}(\mathbf{x}, \boldsymbol{\theta}_s) = \mathbf{f}(\mathbf{x}, \boldsymbol{\theta}_*) + \mathbf{J}_{\boldsymbol{\theta}_*}(\mathbf{x})(\boldsymbol{\theta} - \boldsymbol{\theta}_*)$ is the linearized neural network at $\boldsymbol{\theta}_*$, and $\boldsymbol{\theta}_s \sim q(\boldsymbol{\theta} | \mathcal{D}, \mathcal{M}_*)$.

In all experiments, we optimize the precision parameter $\delta_l > 0$ of a Gaussian prior $\mathcal{N}(0, \delta_l^{-1} \mathbf{I}_l)$ for the weights and biases of each layer l individually and initialize all δ to 1. In regression experiments, we additionally optimize the Gaussian observation noise. We use ADAM (Kingma & Ba, 2015) to optimize the hyperparameters during training with default settings but a higher learning rate between 0.01 and 1 (cf. Sec. 3.4). We optimize the network parameters using ADAM except for the ResNet experiments, where we follow common practice and use SGD with momentum of 0.9. On the image classification datasets, train for 300 epochs in total and decay the learning rate by a factor of 0.1 (He et al., 2016) after 150, 225, and 275 epochs, respectively.

4.1. Illustrative examples

First, we illustrate our model selection approach on simple regression (Fig. 1) and classification (Fig. 3) examples.

Regression. For the regression example we consider the modified Snelson dataset (Snelson, 2007; Khan et al., 2019), see Fig. 1. We run Alg. 1 for two different architectures (1 and 3 hidden layers, 50 neurons per layer) with a step size of 0.01 for parameters and hyperparameters and recompute the marginal likelihood after each epoch ($F = 1$) and with no burn-in ($B = 0$) for 1000 epochs with $K = 1$ hyperparameter updates per step. We use the Laplace-GGN with a full GGN determinant and compute the Bayesian predictive in Eq. 11 based on the optional Laplace-GGN approximation.

The larger network ($P = 5221$ parameters) fits the data well and does not overfit due to the optimized regularization (Fig. 1 (left)). In contrast, the smaller network ($P = 151$ parameters) underfits the data due to its limited capacity and explains parts of the sinusoidal signal with a higher predic-

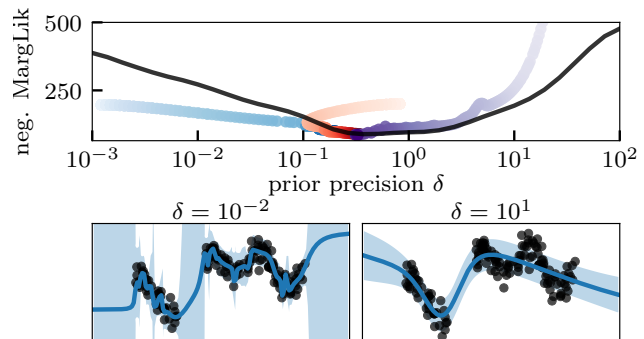


Figure 4: Selection of the prior precision δ for a 3-layer network using the marginal likelihood. *Top*: Three optimization traces (init δ_{init} final) of the online algorithm compared to a grid-search with fixed δ (—). The online algorithm is initialized with three different prior precisions $\delta_{\text{init}} \in \{10^{-3}(\bullet), 1(\bullet), 10^2(\bullet)\}$ and converges to the optimum as found by the grid-search within the same number of steps. *Bottom*: Predictive distributions of an over- and underfitting model, respectively. The predictive of the best model is depicted in Fig. 1 (left). The marginal likelihood correctly identifies the model that agrees with intuition.

tive uncertainty (Fig. 1 (right)). The marginal likelihood identifies the better model. In App. C.1, we show in addition how the resulting Bayesian predictive decomposes into *epistemic* and *aleatoric* uncertainty. Such a decomposition is only possible with optimized hyperparameters and would require a large grid-search without our online method (Khan et al., 2019).

The larger model has enough capacity to overfit on this dataset. To illustrate the marginal likelihood’s ability to select the right amount of regularization and to test the stability of our algorithm, we perform a grid search over the prior precision for the larger network and compare the selected hyperparameters. The online algorithm reliably converges to the same optimum also identified by comparing the marginal likelihood over the grid search after training (optimization traces in Fig. 4 (top)). Moreover, the marginal likelihood correctly identifies the value with the best generalization performance (test log likelihood in App. C.1); choosing hyperparameter values that correspond to worse marginal likelihoods results in overfitting or underfitting respectively, see the predictive distributions in Fig. 4 (bottom) and compare them to the optimal solution in Fig. 1 (left).

Classification. For binary classification, we consider a subsampled ($N = 265$ data points) version of the synthetic 2D banana dataset (Rätsch et al., 2001). We train the same neural network (1 hidden layer with 50 neurons) twice: once with our online algorithm for 200 steps with otherwise same settings as for the regression example above; and a second time with a weakly regularized prior akin to regular deep learning training. The optimization trace and the evolution

Dataset	cross-validation (CV)			MargLik optimization		
	MAP	VI	Laplace	GGN	EF	KFAC
boston	2.71±0.10	2.58±0.03	2.57±0.05	2.69±0.12	2.62±0.12	2.70±0.09
concrete	3.17±0.04	3.17±0.01	3.05±0.04	3.06±0.05	3.07±0.04	3.13±0.06
energy	1.02±0.05	1.42±0.01	0.82±0.03	0.55±0.11	0.73±0.15	0.53±0.02
kin8nm	-1.09±0.01	-0.87±0.00	- 1.23±0.01	-1.14±0.01	-1.14±0.01	-1.13±0.01
naval	-5.75±0.05	-3.82±0.02	-6.40±0.06	- 6.93±0.03	- 6.92±0.04	-6.88±0.05
power	2.82±0.01	2.86±0.01	2.83±0.01	2.78±0.02	2.78±0.01	2.78±0.02
wine	0.98±0.02	0.96±0.01	0.97±0.02	0.93±0.02	0.93±0.01	0.94±0.02
yacht	2.30±0.02	1.67±0.01	1.01±0.05	5.89±1.25	2.43±0.61	1.48±0.07

Table 1: Negative test log likelihood (lower is better) on the UCI regression benchmark. Three leftmost columns: cross-validation (CV) using MAP, VI and Laplace predictives; three rightmost columns: our proposed method with GGN, EF, and GGN-KFAC approximation to the marginal likelihood and MAP predictive. Even compared to VI and Laplace with CV (second and third column), the MAP predictions obtained with our method perform on par or better except on the kin8nm and yacht datasets. The full GGN approximation performs the best, followed by the EF and Kronecker Laplace-GGN approximations. The cross-validation results are taken from Foong et al. (2019). Results within one standard error of the best performance are in bold. Additional results with diagonal GGN and EF as well as Bayesian predictive are in App. C.

of the hyperparameters (softmax temperature as well as prior precision per layer) for our online algorithm is shown in Fig. 3 (left).

The weakly regularized model overfits and has a large generalization gap with a very high accuracy of almost 100% on the train set but only 86% on the test set (Fig. 3, Step 2 (right)). In contrast, our online method reduces this gap and increases the test accuracy to 89% by optimizing the hyperparameters during training using the marginal likelihood (Fig. 3, Step 2 (left)). The optional Bayesian predictive also profits from the optimized hyperparameters (Fig. C.1b). A comparison of the marginal likelihood estimates after training correctly identifies the model with smaller generalization gap and better test performance.

4.2. UCI regression

We compare our method to cross-validation on eight UCI (Dua & Graff, 2017) regression datasets following Hernández-Lobato & Adams (2015) and Foong et al. (2019). In this setup, each dataset is split into 90% training and 10% testing data and a neural network with a single hidden layer, 50 neurons, and a ReLU activation is used. We use the hand-tuned and cross-validated results reported by Foong et al. (2019) who compare MAP, variational inference, and the Laplace approximation. They use 10% of the training data for validation and optimize hyperparameters by grid-search. We run Alg. 1 for 10,000 epochs until convergence with the standard learning rate of ADAM for both hyperparameters and parameters, and set frequency $F = 1$, $K = 1$ hyperparameter gradient steps, and do not use burn-in. We compute standard errors over 10 random splits.

The results in Table 1 indicate that our online algorithm overall performs better than cross-validated baselines in terms of the test log likelihood. Using the simple and efficient

MAP predictive, our method outperforms or matches the Bayesian predictions with cross-validated hyperparameters on 6 out of 8 datasets. Our algorithm performs similarly using the full GGN or EF, and the Kronecker-factored GGN performs almost as good as the full GGN. See App. C.2 and App. C.3 for further details and results on UCI classification datasets, including diagonal GGN and EF approximations. Perhaps surprisingly, the diagonal approximations are effective and also competitive with cross-validation. We further find that our method can alleviate the need for the posterior predictive as it achieves the same performance using only the MAP predictive (performance comparison in App. C.2).

4.3. Image classification

We benchmark our online model selection against cross-validation on standard image classification datasets (MNIST, FMNIST, CIFAR-10, CIFAR-100) and use the resulting marginal likelihood estimate to compare architectures. We compare fully-connected (MLP), convolutional (CNN), and residual (ResNet) networks. Our algorithm is robust to the selection of its hyperparameters (F, K, B, γ , see Sec. 3 and App. C.6). Here, we use our online model selection step every $F = 10$ epochs for $K = 100$ hyperparameter steps without burn-in and with step size $\gamma = 1$ to keep computational overhead low. Due to the size of the datasets and models, we use the Kronecker-factored GGN approximation and the diagonal EF and GGN variants. For the baseline, we use the results and architectures by Immer et al. (2021) who optimized the prior precision using cross-validation, except for the ResNet on CIFAR-10 where we use the hyperparameters of Zhang et al. (2019b). For ResNets, we use fixup (Zhang et al., 2019b) instead of batchnorm because batchnorm conflicts with a Gaussian prior (Zhang et al., 2019a). To estimate standard errors, we run for 5 different random initializations.

Dataset	Model	cross-validation		marginal likelihood optimization					
		accuracy	logLik	accuracy	KFAC logLik	MargLik	diagonal EF		
							accuracy	logLik	MargLik
MNIST	MLP	98.22	-0.061	98.38	-0.053	-0.158	97.05	-0.095	-0.553
	CNN	99.40	-0.017	99.46	-0.016	-0.064	99.45	-0.019	-0.134
FMNIST	MLP	88.09	-0.347	89.83	-0.305	-0.468	85.72	-0.400	-0.756
	CNN	91.39	-0.258	92.06	-0.233	-0.401	91.69	-0.233	-0.570
CIFAR10	CNN	77.41	-0.680	80.46	-0.644	-0.967	80.17	-0.600	-1.359
	ResNet	83.73	-1.060	86.11	-0.595	-0.717	85.82	-0.464	-0.876

Table 2: Model selection by marginal likelihood compared with cross-validation on image classification. We report the test accuracy, test log likelihood (logLik), and log marginal likelihood (MargLik). Higher is better for all metrics. Generally, models selected by our method perform better than the cross-validated models, in particular on CIFAR-10. More importantly, higher accuracies correspond to higher marginal-likelihood. The marginal likelihood agrees with the intuition that CNNs are better than MLPs and ResNets are better than CNNs. Performance reported over 5 random initializations, best performance per dataset within one standard error in bold. Cross-validation results on CNN and MLP are taken from Immer et al. (2021). Results with standard errors and performance of diagonal GGN are reported in App. C.4.

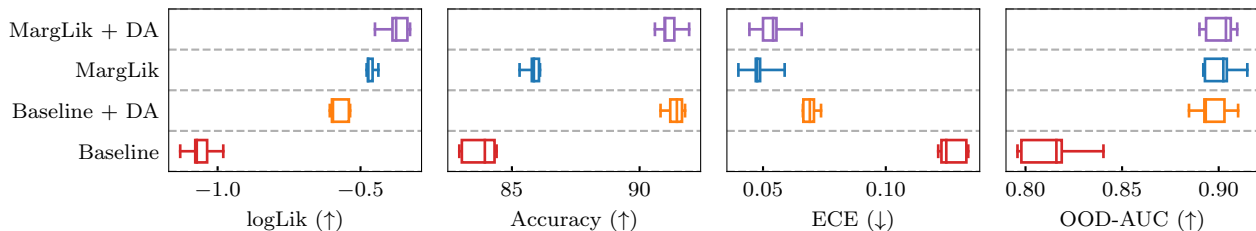


Figure 5: Comparison to a baseline on the ResNet-20 architecture with and without data augmentation (*DA*) on CIFAR-10. We report test log-likelihood (logLik), test accuracy, expected calibration error (ECE), and out-of-distribution (OOD) detection performance in terms of area under the ROC (*OOD-AUC*) using the SVHN validation set as OOD data. Arrows indicate if higher (↑) or lower (↓) values are better. Even without data augmentation, our MargLik-based method achieves a logLik, ECE, and OOD-AUC better than the baseline with data augmentation. Our approach paired with data augmentation slightly improves on that and matches the accuracy obtained by the baseline with data augmentation.

The results in Table 2 show that our method improves the performance over baselines on the considered architectures with the largest improvement on CIFAR-10. We find that the Kronecker-factored version is well-suited for fully-connected networks but the diagonal variants are often sufficient, on CIFAR-10 even slightly better, for convolutional neural networks. The resulting marginal likelihood estimates of any method suggest that CNNs are better suited for image classification than MLPs, and on CIFAR-10 we further see that ResNets are superior to standard CNNs without residual connections. In App. C.4, we additionally show the outcome with the diagonal GGN and list standard errors.

In Fig. 5, we show results with additional data augmentation on CIFAR-10 and ResNet architecture and report two additional performance metrics. Here, we display the diagonal EF approximation due to its effectiveness (performance of Kronecker-factored variant in App. C.4). Additionally to accuracy and negative log likelihood, we show the expected calibration error (*ECE*, Guo et al. (2017)) and out-of-distribution detection performance in terms of area under the receiver-operator curve (*OOD-AUC*). With and without data

augmentation, the models trained with our method achieve better test log-likelihood (*NLL*), expected calibration error (*ECE*), and out-of-distribution detection performance. Compared to the baseline, the performance can be up to $2\times$ better using our method. Notably, our method achieves a better *NLL*, *ECE*, and similar *OOD-AUC* *without* data augmentation than the baseline *with* data augmentation. However, the baseline can mitigate the difference in accuracy by data augmentation and match the performance on our method. Following Osawa et al. (2019), we upweight the likelihood by a factor of 5 to account for the data augmentation.

In Fig. 6, we show that the proposed online model selection can improve over a baseline with weight decay by greatly reducing overfitting and the generalization gap on CIFAR-10. Compared to a single training run that uses fixed hyperparameters, our online method only takes around twice the time for training when using the Kronecker-factored Laplace-GGN every $F = 10$ epochs. Cross-validation would only be able to explore two parameter settings in this time.

Finally, we conduct a larger-scale study for architecture

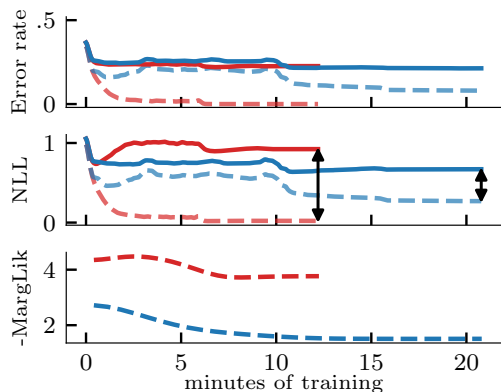


Figure 6: Train (---) vs. test (—) performance of our method (—) compared to a baseline with default weight decay (---) for a CNN on CIFAR-10. Online marginal likelihood optimization leads to a smaller generalization gap (\longleftrightarrow). While the test error rate matches, the baseline has a significantly worse negative log likelihood. The Laplace-GGN marginal likelihood estimate in the bottom indicates that as well. The Kronecker-factored Laplace-GGN approximation increases the training time only by a factor of 2. For cross-validation, this would only suffice to retrain for two different hyperparameters.

selection after training (step 2 in Sec. 3) by applying our algorithm to various architectures and comparing the resulting marginal likelihood estimates. We use the algorithm with the diagonal EF approximation due to its efficiency and optimize the prior precision hyperparameter for each layer.¹ After training, we use the final marginal likelihood estimates to rank the different architectures. On CIFAR-10 and CIFAR-100, we train CNNs and ResNets of varying width (between 2 and 64) and depth (between 1 and 110). On FashionMNIST, we compare CNNs and MLPs. For each data set, we compare around 40 models. In Fig. 2, each trained model with our method is represented by a marker whose size and color depends on the number of parameters. On CIFAR-10/100, ResNets achieve higher marginal likelihoods than CNNs despite, in some cases, exponentially more parameters. In terms of architecture, width tends to improve marginal likelihood more than depth (see Fig. 7 and App. C.5). This is in line with improved ResNet architectures that use increased width (Zagoruyko & Komodakis, 2016). On both data sets, the rank correlation between test accuracy and marginal likelihood is 97% in terms of Spearman’s ρ . Spearman’s ρ measures the correlation of the model rankings that test accuracy and marginal likelihood induce (Kendall, 1948). CNNs achieve consistently higher marginal likelihoods than MLPs on FMNIST. Especially at similar performance, CNNs achieve a higher marginal

¹Similar results can be obtained with the Kronecker-factored variant but at a higher cost.

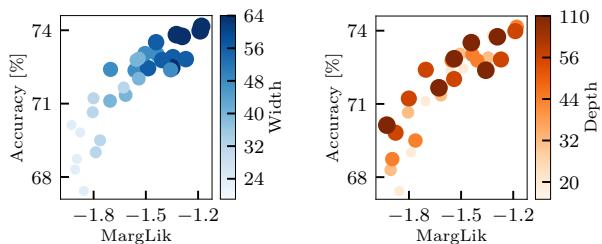


Figure 7: Wider ResNets give both higher marginal-likelihoods and accuracy (left) while there is no clear trend seen by varying depths (right). Results are on CIFAR-100. Each plot contains 30 models. Details in App. C.5

likelihood than MLPs, potentially due to the reduced model complexity. On FMNIST, the rank correlation is 69%. The correlation is likely lower because the marginal likelihood often selects significantly smaller instead of slightly better performing models (see top right in Fig. 2). For more detailed results and the architectures, see App. C.5.

5. Conclusion

In this paper, we present the marginal likelihood as a viable tool for model selection in deep learning. Even after making approximations for scalability, the marginal likelihood faithfully reflects the model quality based on the training data alone. Estimation requires only a mild increase in computation, but allows us to compare models and even select hyperparameters during training. Ultimately, the marginal likelihood and similar methods make use of the neighborhood of a solution to improve their robustness. We believe this is important to design models for applications where little is known about deployment and future usage. Removing dependence on validation data can widen the impact of deep learning and open up new application areas.

Many interesting research directions remain open for exploration. It is important to explore ways to further improve Hessian approximations and computation, and consider other approximate inference methods. Online model selection for discrete hyperparameters is another interesting direction. Finally, extending this work beyond supervised learning, e.g., to bandits, Bayesian optimization, active learning, or continual learning, is an important avenue for future research. We hope that this work encourages others to pursue new ideas based on Bayesian model selection.

Acknowledgements

A. I. acknowledges funding by the Max Planck ETH Center for Learning Systems (CLS). M. B. acknowledges funding by the Max Planck Society, the EPSRC, and a Qualcomm European Scholarship in Technology. V. F. acknowledges funding by the Swiss Data Science Center.

References

- Bishop, C. M. *Pattern recognition and machine learning*. Information Science and Statistics. Springer, 2006.
- Blumer, A., Ehrenfeucht, A., Haussler, D., and Warmuth, M. K. Occam’s razor. *Information processing letters*, 24(6):377–380, 1987.
- Blundell, C., Cornebise, J., Kavukcuoglu, K., and Wierstra, D. Weight uncertainty in neural networks. In *Proceedings of the 32nd International Conference on Machine Learning*, pp. 1613–1622, 2015.
- Botev, A., Ritter, H., and Barber, D. Practical Gauss-Newton optimisation for deep learning. In *International Conference on Machine Learning*, International Convention Centre, Sydney, Australia, 2017. PMLR.
- Bottou, L. Large-scale machine learning with stochastic gradient descent. In *Proceedings of COMPSTAT’2010*, pp. 177–186. Springer, 2010.
- Buntine, W. L. and Weigend, A. S. Bayesian back-propagation. *Complex systems*, 5(6):603–643, 1991.
- Damianou, A. and Lawrence, N. D. Deep Gaussian processes. In *Proceedings of the Sixteenth International Conference on Artificial Intelligence and Statistics*. PMLR, 2013.
- Dangel, F., Kunstner, F., and Hennig, P. Backpack: Packing more into backpack. In *Proceedings of 7th International Conference on Learning Representations*, 2019.
- Dua, D. and Graff, C. UCI machine learning repository, 2017. URL <http://archive.ics.uci.edu/ml>.
- Dutordoir, V., van der Wilk, M., Artemev, A., and Hensman, J. Bayesian image classification with deep convolutional gaussian processes. In *Proceedings of the Twenty Third International Conference on Artificial Intelligence and Statistics*, 2020.
- Dziugaite, G. K. and Roy, D. M. Computing nonvacuous generalization bounds for deep (stochastic) neural networks with many more parameters than training data. *arXiv preprint arXiv:1703.11008*, 2017.
- Fong, E. and Holmes, C. On the marginal likelihood and cross-validation. *Biometrika*, 107(2):489–496, 2020.
- Foong, A. Y., Li, Y., Hernández-Lobato, J. M., and Turner, R. E. ‘in-between’ uncertainty in bayesian neural networks. *arXiv preprint arXiv:1906.11537*, 2019.
- Foresee, F. D. and Hagan, M. T. Gauss-newton approximation to bayesian learning. In *International Conference on Neural Networks (ICNN’97)*, volume 3, pp. 1930–1935. IEEE, 1997.
- Guo, C., Pleiss, G., Sun, Y., and Weinberger, K. Q. On calibration of modern neural networks. In *International Conference on Machine Learning*, pp. 1321–1330. PMLR, 2017.
- Harville, D. A. Matrix algebra from a statistician’s perspective, 1998.
- He, K., Zhang, X., Ren, S., and Sun, J. Deep residual learning for image recognition. In *2016 IEEE Conference on Computer Vision and Pattern Recognition, CVPR 2016, Las Vegas, NV, USA, June 27-30, 2016*, pp. 770–778. IEEE Computer Society, 2016.
- Hernández-Lobato, J. M. and Adams, R. Probabilistic back-propagation for scalable learning of bayesian neural networks. In *International Conference on Machine Learning*, pp. 1861–1869. PMLR, 2015.
- Hochreiter, S. and Schmidhuber, J. Flat minima. *Neural Computation*, 9(1):1–42, 1997.
- Immer, A., Korzepa, M., and Bauer, M. Improving predictions of bayesian neural nets via local linearization. In *Proceedings of The 24th International Conference on Artificial Intelligence and Statistics*, pp. 703–711, 2021.
- Jefferys, W. H. and Berger, J. O. Ockham’s razor and bayesian analysis. *American Scientist*, 80(1):64–72, 1992. ISSN 00030996.
- Jiang, Y., Neyshabur, B., Mobahi, H., Krishnan, D., and Bengio, S. Fantastic generalization measures and where to find them. In *International Conference on Learning Representations*, 2019.
- Kendall, M. G. Rank correlation methods. 1948.
- Keskar, N. S., Mudigere, D., Nocedal, J., Smelyanskiy, M., and Tang, P. T. P. On large-batch training for deep learning: Generalization gap and sharp minima. *arXiv preprint arXiv:1609.04836*, 2016.
- Khan, M., Nielsen, D., Tangkaratt, V., Lin, W., Gal, Y., and Srivastava, A. Fast and scalable bayesian deep learning by weight-perturbation in adam. In *International Conference on Machine Learning*, pp. 2611–2620, 2018.
- Khan, M. E. E., Immer, A., Abedi, E., and Korzepa, M. Approximate inference turns deep networks into gaussian processes. In *Advances in Neural Information Processing Systems*, pp. 3088–3098, 2019.
- Kingma, D. P. and Ba, J. Adam: A method for stochastic optimization. In *International Conference on Learning Representations*, 2015.

- Kristiadi, A., Hein, M., and Hennig, P. Being bayesian, even just a bit, fixes overconfidence in relu networks. In *International Conference on Machine Learning*, pp. 5436–5446. PMLR, 2020.
- Kunstner, F., Hennig, P., and Balles, L. Limitations of the empirical fisher approximation for natural gradient descent. In *Advances in Neural Information Processing Systems*, pp. 4158–4169, 2019.
- Lakshminarayanan, B., Pritzel, A., and Blundell, C. Simple and scalable predictive uncertainty estimation using deep ensembles. In *Advances in neural information processing systems*, pp. 6402–6413, 2017.
- Llorente, F., Martino, L., Delgado, D., and Lopez-Santiago, J. Marginal likelihood computation for model selection and hypothesis testing: an extensive review. *arXiv preprint arXiv:2005.08334*, 2020.
- Lyle, C., Schut, L., Ru, R., Gal, Y., and van der Wilk, M. A bayesian perspective on training speed and model selection. *Advances in Neural Information Processing Systems*, 33, 2020.
- MacKay, D. J. A practical bayesian framework for backpropagation networks. *Neural computation*, 4(3):448–472, 1992.
- MacKay, D. J. Probable networks and plausible predictions—a review of practical bayesian methods for supervised neural networks. *Network: computation in neural systems*, 6(3):469–505, 1995.
- MacKay, D. J. *Information theory, inference and learning algorithms*. Cambridge university press, 2003.
- Maddox, W. J., Izmailov, P., Garipov, T., Vetrov, D. P., and Wilson, A. G. A simple baseline for bayesian uncertainty in deep learning. In *Advances in Neural Information Processing Systems*, pp. 13132–13143, 2019.
- Martens, J. and Grosse, R. Optimizing neural networks with kronecker-factored approximate curvature. In *International conference on machine learning*, pp. 2408–2417, 2015.
- Mascarenhas, W. F. The divergence of the bfgs and gauss newton methods. *Mathematical Programming*, 147(1): 253–276, 2014.
- Neal, R. M. *Bayesian Learning for Neural Networks*. PhD thesis, University of Toronto, 1995.
- Neyman, J. and Pearson, E. S. IX. on the problem of the most efficient tests of statistical hypotheses. *Philosophical Transactions of the Royal Society of London. Series A, Containing Papers of a Mathematical or Physical Character*, 231(694-706):289–337, 1933.
- Osawa, K., Swaroop, S., Khan, M. E. E., Jain, A., Eschenhagen, R., Turner, R. E., and Yokota, R. Practical deep learning with bayesian principles. In *Advances in Neural Information Processing Systems*, pp. 4289–4301, 2019.
- Rasmussen, C. E. and Ghahramani, Z. Occam’s razor. In *Advances in neural information processing systems*, pp. 294–300, 2001.
- Rasmussen, C. E. and Williams, C. K. *Gaussian processes for machine learning*. MIT press Cambridge, MA, 2006.
- Rätsch, G., Onoda, T., and Müller, K.-R. Soft margins for adaboost. *Machine learning*, 42(3):287–320, 2001.
- Ritter, H., Botev, A., and Barber, D. A scalable laplace approximation for neural networks. In *International Conference on Learning Representations*, 2018.
- Robbins, H. *An empirical Bayes approach to statistics*. Office of Scientific Research, US Air Force, 1955.
- Schneider, F., Balles, L., and Hennig, P. Deepobs: A deep learning optimizer benchmark suite. In *International Conference on Learning Representations*, 2018.
- Snelson, E. L. *Flexible and efficient Gaussian process models for machine learning*. PhD thesis, UCL (University College London), 2007.
- van der Wilk, M., Bauer, M., John, S., and Hensman, J. Learning invariances using the marginal likelihood. In *Advances in Neural Information Processing Systems*, pp. 9938–9948, 2018.
- Wenzel, F., Roth, K., Veeling, B. S., Światkowski, J., Tran, L., Mandt, S., Snoek, J., Salimans, T., Jenatton, R., and Nowozin, S. How good is the bayes posterior in deep neural networks really? In *International Conference on Machine Learning*, 2020.
- Zagoruyko, S. and Komodakis, N. Wide residual networks. In *BMVC*. BMVA Press, 2016.
- Zhang, G., Sun, S., Duvenaud, D., and Grosse, R. Noisy natural gradient as variational inference. In *International Conference on Machine Learning*, pp. 5852–5861, 2018.
- Zhang, G., Wang, C., Xu, B., and Grosse, R. B. Three mechanisms of weight decay regularization. In *ICLR (Poster)*. OpenReview.net, 2019a.
- Zhang, H., Dauphin, Y. N., and Ma, T. Fixup initialization: Residual learning without normalization. In *International Conference on Learning Representations*, 2019b.

Scalable Marginal Likelihood Estimation for Model Selection in Deep Learning (Appendix)

A. Derivations and additional details

A.1. Laplace approximation to the marginal likelihood

We briefly derive the Laplace approximation to the marginal likelihood and discuss the additional correction term that would arise in online estimation. We derive the local Laplace approximation at an arbitrary point θ_* similar to the standard Laplace approximation by a local quadratic approximation. Recall the Hessian $\mathbf{H}_\theta = -\nabla_{\theta\theta}^2 \log p(\mathcal{D}, \theta | \mathcal{M})$ and define the gradient $\mathbf{g}_\theta = -\nabla_\theta \log p(\mathcal{D}, \theta | \mathcal{M})$ of the MAP objective in Eq. 6. A second-order Taylor approximation around θ_* to the log joint distribution is then given by

$$\log p(\mathcal{D}, \theta | \mathcal{M}) \approx \log p(\mathcal{D}, \theta_* | \mathcal{M}) - (\theta - \theta_*)^\top \mathbf{g}_{\theta_*} - \frac{1}{2} (\theta - \theta_*)^\top \mathbf{H}_{\theta_*} (\theta - \theta_*). \quad (\text{A.1})$$

In the standard Laplace approximation, the second term disappears due to $\mathbf{g}_{\theta_*} = \mathbf{0}$. We compute the Laplace approximation to the marginal likelihood by solving the integral in Eq. 1 using the above approximation to the log joint:

$$\begin{aligned} p(\mathcal{D} | \mathcal{M}) &= \int p(\mathcal{D}, \theta | \mathcal{M}) \, d\theta \\ &\approx \int \exp \left[\log p(\mathcal{D}, \theta_* | \mathcal{M}) - (\theta - \theta_*)^\top \mathbf{g}_{\theta_*} - \frac{1}{2} (\theta - \theta_*)^\top \mathbf{H}_{\theta_*} (\theta - \theta_*) \right] \, d\theta \\ &= p(\mathcal{D}, \theta_* | \mathcal{M}) \int \exp \left[-(\theta - \theta_*)^\top \mathbf{g}_{\theta_*} - \frac{1}{2} (\theta - \theta_*)^\top \mathbf{H}_{\theta_*} (\theta - \theta_*) \right] \, d\theta \\ &= p(\mathcal{D}, \theta_* | \mathcal{M}) \int \exp \left[-\frac{1}{2} (\theta - \theta_* + \mathbf{H}_{\theta_*}^{-1} \mathbf{g}_{\theta_*})^\top \mathbf{H}_{\theta_*} (\theta - \theta_* + \mathbf{H}_{\theta_*}^{-1} \mathbf{g}_{\theta_*}) + \frac{1}{2} \mathbf{g}_{\theta_*}^\top \mathbf{H}_{\theta_*}^{-1} \mathbf{g}_{\theta_*} \right] \, d\theta \\ &= p(\mathcal{D}, \theta_* | \mathcal{M}) \exp \left(\frac{1}{2} \mathbf{g}_{\theta_*}^\top \mathbf{H}_{\theta_*}^{-1} \mathbf{g}_{\theta_*} \right) \int \exp \left[-\frac{1}{2} (\theta - \theta_* + \mathbf{H}_{\theta_*}^{-1} \mathbf{g}_{\theta_*})^\top \mathbf{H}_{\theta_*} (\theta - \theta_* + \mathbf{H}_{\theta_*}^{-1} \mathbf{g}_{\theta_*}) \right] \, d\theta \\ &= p(\mathcal{D}, \theta_* | \mathcal{M}) \exp \left(\frac{1}{2} \mathbf{g}_{\theta_*}^\top \mathbf{H}_{\theta_*}^{-1} \mathbf{g}_{\theta_*} \right) (2\pi)^{\frac{p}{2}} |\mathbf{H}_{\theta_*}|^{-\frac{1}{2}}. \end{aligned}$$

To obtain this result, we first complete the square inside the exponent:

$$\begin{aligned} -(\theta - \theta_*)^\top \mathbf{g}_{\theta_*} - \frac{1}{2} (\theta - \theta_*)^\top \mathbf{H}_{\theta_*} (\theta - \theta_*) &= - \left[(\theta - \theta_*)^\top \mathbf{g}_{\theta_*} + \frac{1}{2} (\theta - \theta_*)^\top \mathbf{H}_{\theta_*} (\theta - \theta_*) \right] \\ &= - \left[\frac{1}{2} (\theta - \theta_* + \mathbf{H}_{\theta_*}^{-1} \mathbf{g}_{\theta_*})^\top \mathbf{H}_{\theta_*} (\theta - \theta_* + \mathbf{H}_{\theta_*}^{-1} \mathbf{g}_{\theta_*}) - \frac{1}{2} \mathbf{g}_{\theta_*}^\top \mathbf{H}_{\theta_*}^{-1} \mathbf{g}_{\theta_*} \right]. \end{aligned} \quad (\text{A.2})$$

The last step is to solve the Gaussian integral which gives the remaining factors $(2\pi)^{\frac{p}{2}} |\mathbf{H}_{\theta_*}|^{-\frac{1}{2}}$. Taking the log, we obtain the log marginal likelihood approximation presented in Eq. 3 with an additional correction term $\frac{1}{2} \mathbf{g}_{\theta_*}^\top \mathbf{H}_{\theta_*}^{-1} \mathbf{g}_{\theta_*}$. We empirically found that the correction term does not help during the online algorithm. For example see Fig. 6, where the marginal likelihood estimation remains stable during training without a correction term. However, the correction term could be computed as efficiently as the determinants we require for our algorithm. We believe the reason for its worse performance is due to an undesired change of the neural network parameter θ_* to $\theta_* + \mathbf{H}_{\theta_*}^{-1} \mathbf{g}_{\theta_*}$. The parameter change is due to the integration over θ of Eq. A.2, which yields a local Laplace approximation to the posterior with mean $\mu = \theta_* + \mathbf{H}_{\theta_*}^{-1} \mathbf{g}_{\theta_*}$. This parameter update resembles a *full* step of Newton's method and does typically lead to divergence (Mascarenhas, 2014), except, for example, in linear least squares. We therefore ignore the correction term and treat the current parameter as θ_* . It is common to assume the gradient is zero, i.e., $\mathbf{g}_{\theta_*} = \mathbf{0}$, when using the Laplace approximation in deep learning (Ritter et al., 2018; Kristiadi et al., 2020). We follow this simplification with our online approximation.

A.2. Efficient determinant computation

We can make the computation of the log determinant more efficient using Woodbury’s identity and the same idea applies to the correction term in the local Laplace approximation. The local Laplace approximation relies on terms that involve expensive computations with the Hessian \mathbf{H}_θ which we approximate either by the GGN or EF. That is, we have either $\mathbf{H} \approx \mathbf{J}_\theta^\top \mathbf{L}_\theta \mathbf{J}_\theta + \mathbf{P}_\theta$ (GGN) or $\mathbf{H} \approx \mathbf{G}_\theta^\top \mathbf{G}_\theta + \mathbf{P}_\theta$ (EF). The results for the determinant are already presented in Eq. 8 and a proof can be found in the literature, e.g., see Theorem 18.1.1 by Harville (1998). For the correction term, we can similarly shift the computational complexity from the number of parameters to the number of data points. This can be achieved by standard application of Woodbury’s matrix identity; see for example Theorem 18.2.8 by Harville (1998).

A.3. Kronecker-factored Laplace-GGN without damping

Kronecker-factored Laplace typically uses *damping* to combine a Gaussian prior with the Hessian approximation (Ritter et al., 2018). When using damping, the log likelihood Hessian and log prior Hessian are not added but also multiplied, which distorts the Laplace approximation. In particular because we optimize the prior parameters, such a distortion is likely to be problematic. We will first discuss damping and how we can compute the log determinant efficiently without damping, before presenting ablation results on image classification which suggest that damping should be avoided in this context.

Kronecker-factored Laplace approximates the GGN using two Kronecker factors, i.e., we have $[\mathbf{J}_\theta^\top \mathbf{L}_\theta \mathbf{J}_\theta]_l \approx \mathbf{Q}_l \otimes \mathbf{W}_l$ where l denotes the index of a single layer. \mathbf{Q}_l is quadratic in the number of neurons of the l -th layer while \mathbf{W}_l is quadratic in the number of neurons of the previous layer (Botev et al., 2017). We assume an isotropic prior for the corresponding layer with $[\mathbf{P}_\theta]_l = p_\theta^{(l)} \mathbf{I}_l$. Then, the Laplace approximation with damping yields

$$[\mathbf{H}_\theta^{\text{GGN}}]_l \approx \mathbf{Q}_l \otimes \mathbf{W}_l + p_\theta^{(l)} \mathbf{I}_l \approx (\mathbf{Q}_l + \sqrt{p_\theta^{(l)}} \mathbf{I}) \otimes (\mathbf{W}_l + \sqrt{p_\theta^{(l)}} \mathbf{I}), \quad (\text{A.3})$$

where \mathbf{I} are of matching size. Clearly, the prior $p_\theta^{(l)}$ is now multiplied by the Kronecker factors and the update is not purely additive anymore. However, it is equally efficient to compute the determinant of the Kronecker approximation without damping. We use the eigendecomposition of $\mathbf{Q}_l \otimes \mathbf{W}_l$ which can be written as $\mathbf{M}_l(\text{diag}(\mathbf{q}^{(l)}) \otimes \text{diag}(\mathbf{w}^{(l)}))\mathbf{M}_l^\top$, where \mathbf{M}_l is the eigenbase of the Kronecker product and $\mathbf{q}^{(l)}$ and $\mathbf{w}^{(l)}$ are vectors of eigenvalues of \mathbf{Q}_l and \mathbf{W}_l as defined before in Sec. 3. The $\text{diag}(\cdot)$ operator turns a vector into a diagonal matrix with the corresponding vector as diagonal. The determinant for the GGN of one layer can be computed using properties of the Kronecker product and determinant:

$$\begin{aligned} |[\mathbf{H}_\theta^{\text{GGN}}]_l| &\approx |\mathbf{Q}_l \otimes \mathbf{W}_l + p_\theta^{(l)} \mathbf{I}_l| = |\mathbf{M}_l(\text{diag}(\mathbf{q}^{(l)}) \otimes \text{diag}(\mathbf{w}^{(l)}))\mathbf{M}_l^\top + p_\theta^{(l)} \mathbf{I}_l| \\ &= |\mathbf{M}_l(\text{diag}(\mathbf{q}^{(l)}) \otimes \text{diag}(\mathbf{w}^{(l)}) + p_\theta^{(l)} \mathbf{I}_l)\mathbf{M}_l^\top| = |\text{diag}(\mathbf{q}^{(l)}) \otimes \text{diag}(\mathbf{w}^{(l)}) + p_\theta^{(l)} \mathbf{I}| \\ &= \prod_{ij} \mathbf{q}_i^{(l)} \mathbf{w}_j^{(l)} + p_\theta^{(l)}. \end{aligned}$$

To compute the final term, we only need the eigenvalues of both Kronecker factors and perform an outer product over the number of input and output neurons. The entire determinant is simply a product over the l layers due to the block-diagonal structure. The expression is given in Eq. 9.

We empirically compare the proposed version to the damped version and find that it is indeed necessary to use the exact version. The performance of the online algorithm using a damped Kronecker-factored Laplace-GGN yields significantly worse results with negative likelihoods up to two times worse. The accuracy suffers as well with a decrease of up to 4% points. Table A1 contains the results for the same experimental setup as described in Sec. 4 and Table 2.

Dataset	Model	accuracy	KFAC		accuracy	KFAC damped	
			logLik	MargLik		logLik	MargLik
MNIST	MLP	98.38±0.04	-0.053±0.002	-0.158±0.001	95.89±0.11	-0.141±0.004	-2.199±0.008
MNIST	CNN	99.46±0.01	-0.016±0.001	-0.064±0.000	98.78±0.09	-0.040±0.002	-1.022±0.017
FMNIST	MLP	89.83±0.14	-0.305±0.006	-0.468±0.002	84.12±0.23	-0.444±0.008	-2.022±0.026
FMNIST	CNN	92.06±0.10	-0.233±0.004	-0.401±0.001	89.54±0.10	-0.296±0.003	-2.424±0.013
CIFAR10	CNN	80.46±0.10	-0.644±0.010	-0.967±0.003	76.38±0.50	-0.690±0.014	-4.232±0.068

Table A1: Ablation of Kronecker-factored Laplace without and with *damping*: avoiding commonly used damping improves the performance across all experiments when using the online algorithm. Damping should be avoided in this context.

B. Computational details

We discuss the computational considerations necessary to apply the algorithm practically, i.e., to different hyperparameters, with different GGN and EF approximations, and number of hyperparameter updates K . In particular, we discuss the cost of line 6 for estimating the marginal likelihood and lines 7 to 10 for updating the hyperparameters and the marginal likelihood in Alg. 1 for individual Laplace-GGN and EF approximations and choices of differentiable hyperparameters. As detailed in Sec. 3.4, the other parameter settings need to be chosen to enable convergence of the marginal likelihood: the step size γ can be set by monitoring the convergence of the marginal likelihood and hyperparameters, and the update frequency F and number of burn-in epochs B should be set to ensure enough steps for convergence while keeping the computational overhead low. The settings F and B simply impact the number of marginal likelihood estimations.

Recall the neural network model introduced in Sec. 2: we have likelihood $p(\mathcal{D}|\boldsymbol{\theta}, \mathcal{M})$ and prior $p(\boldsymbol{\theta}|\mathcal{M})$, where the model \mathcal{M} consists of hyperparameters that are differentiable in the marginal likelihood and discrete choices. Here, we entirely focus on the hyperparameters that are differentiable in the marginal likelihood. For both regression and classification, we work with an isotropic Gaussian prior per layer ², i.e., $p(\boldsymbol{\theta}|\mathcal{M}) = \prod_l \mathcal{N}(\boldsymbol{\theta}_l|\mathbf{0}, \delta_l^{-1}\mathbf{I}_l)$ where l denotes the layer or group of parameters; we consider the weights and biases of each layer as individual parameter groups l . Hence, the Hessian of the log prior, \mathbf{P}_θ , is diagonal but with blocks of isotropic diagonals per layer l . For regression, we use a Gaussian likelihood and optimize the observation noise variance σ^2 using the marginal likelihood, i.e., we have the likelihood $p(\mathcal{D}|\boldsymbol{\theta}, \mathcal{M}) = \mathcal{N}(\mathbf{y}|\mathbf{f}(\mathbf{x}; \boldsymbol{\theta}), \sigma^2)$. For classification, we only optimize the softmax temperature T in the illustrative example (Fig. 3) and have likelihood $p(\mathcal{D}|\boldsymbol{\theta}, \mathcal{M}) = \text{Categorical}(\mathbf{y}|\text{softmax}(\mathbf{f}(\mathbf{x}; \boldsymbol{\theta})/T))$ since it permits K cheap iterations without requiring re-computing expensive quantities.

We use either the GGN or EF approximation to the marginal likelihood in Eq. 3 at the current neural network parameters $\boldsymbol{\theta}_*$:

$$\log q(\mathcal{D}|\mathcal{M}) = \log p(\mathcal{D}|\boldsymbol{\theta}_*, \mathcal{M}) + \log p(\boldsymbol{\theta}_*|\mathcal{M}) + \frac{P}{2} \log 2\pi - \frac{1}{2} \log \left| \mathbf{H}_{\boldsymbol{\theta}_*}^{\text{GGN/EF}} \right|. \quad (\text{B.1})$$

The first term, the log likelihood, can be computed based on the neural network functions $\mathbf{f}(\mathbf{x}; \boldsymbol{\theta}_*)$ over the entire dataset in $\mathcal{O}(NP)$ but an unbiased estimator in $\mathcal{O}(MP)$ with minibatch M is also possible³. If we update hyperparameters of the log likelihood, for example, in regression, we further store the functions. The second term, the log prior, can be computed based on the current neural network parameters $\boldsymbol{\theta}_*$ in $\mathcal{O}(P)$ for our choice of prior. As outlined in Sec. 3, the major problem, and the only part in which the approximations differ, is to compute the GGN and EF log determinant. In the following, we discuss the cost of one determinant computation with the different approximations and the follow-up cost of K updates and hyperparameter steps. For classification, we deal with $\mathcal{M}^\theta = \{\delta_l\}$ and for regression we additionally have $\sigma^2 \in \mathcal{M}^\theta$.

B.1. Full Laplace-GGN

For the full Laplace-GGN, we need to pass through the training data to compute all Jacobians \mathbf{J}_θ and log-likelihood Hessians \mathbf{L}_θ with complexity $\mathcal{O}(NPC)$ and $\mathcal{O}(NC^2)$, respectively. We can then compute the log determinant in two ways depending on N, P, C . If $P < NC$, we use the standard method: we first compute the $P \times P$ matrix in Eq. 4 in $\mathcal{O}(P^2NC + PNC^2)$. Computing the log determinant of the resulting matrix is then $\mathcal{O}(P^3)$. Otherwise, i.e., if $NC < P$, we use the proposed formulation in Sec. 3, Eq. 8: in this case the computation is $\mathcal{O}(N^2C^2P)$ for construction and $\mathcal{O}(N^3C^3)$ to compute the determinant. Using multiple iterations are in general not cheaper unless we have an isotropic prior and $\mathbf{P}_\theta \propto \mathbf{I}_P$, which is common in Bayesian deep learning. In this case, we can start with an initial eigendecomposition in $\mathcal{O}(P^3)$ or $\mathcal{O}(N^3C^3)$ but then update K times in $\mathcal{O}(P)$ and $\mathcal{O}(N)$, respectively.

B.2. Full Laplace-EF

In comparison to the full Laplace-GGN, the EF-based alternative scales independently of the number of outputs C and therefore typically cheaper and we can trade off between P and N directly. We first need to compute (and store) the individual gradients in $\mathcal{O}(NP)$. If $P < N$, we use the standard version by computing Eq. 5 in $\mathcal{O}(P^2N)$ and then the determinant in $\mathcal{O}(P^3)$. If $N < P$, we use the matrix determinant equivalence in Eq. 8 to reduce computation to $\mathcal{O}(N^2P)$ and determinant computation to $\mathcal{O}(N^3)$. In line with the full Laplace-GGN, multiple iterations are in general not cheaper unless $\mathbf{P}_\theta \propto \mathbf{I}_P$ in which case we can use an initial eigendecomposition of the same complexity and iterate cheaply in $\mathcal{O}(P)$ or $\mathcal{O}(N)$.

²Except for Fig. 4 where we compare against a grid-search which is expensive already for two dimensions and high resolution.

³We assume a standard architecture that allows a forward pass in $\mathcal{O}(P)$

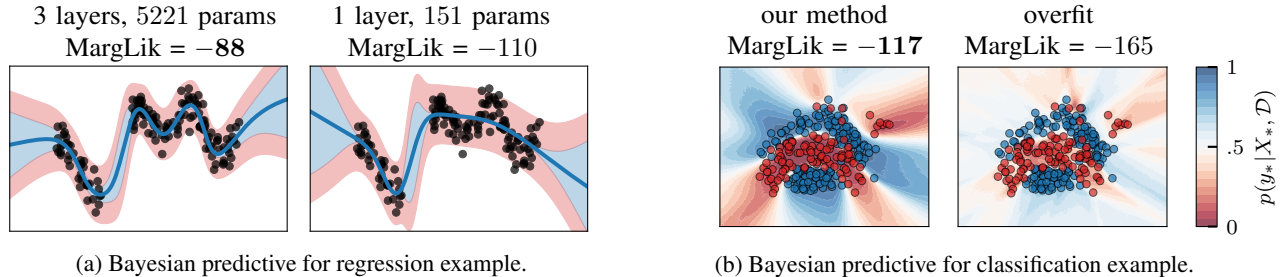


Figure C.1: Optional Bayesian posterior predictives (Eq. 11) as alternative to the MAP predictives (Eq. 12) displayed in Fig. 1 and Fig. 3. (a) Posterior predictive for regression example with noise variance (■) and neural network model uncertainty (■). Marginal likelihood training results in Bayesian predictives with a reasonable split into both uncertainties which is hard to obtain by other means. (b) The posterior predictive for classification example yields a predictive that is certain in the data region and less certain away from it when using marginal likelihood optimization.

B.3. Kronecker-factored Laplace-GGN or EF

The Kronecker-factored Laplace approximations are not only cheaper to compute and store but are also significantly more efficient in updating per-layer hyperparameters due to the per-layer block-diagonal approximation. During the pass through the training data, the Kronecker factors are computed and stored (Botev et al., 2017) which is $\mathcal{O}(NP + N(D^2 + C^2 + \sum_l H_l^2))$ where H_l is the size of the l -th hidden layer. That is because each Kronecker factor is quadratic in the number of neurons of the input or output of some layer. We compute the eigendecomposition of all Kronecker factors in $\mathcal{O}(D^3 C^3 + \sum_l H_l^3)$ but only keep the eigenvalues necessary to compute Eq. 9. Updating the per-layer prior precision and observation noise variance are only $\mathcal{O}(P)$ due to Eq. 9 and many hyperparameter updates help amortize the up-front cost. We compute the Kronecker factors using the backpack package by Dangel et al. (2019).

B.4. Diagonal Laplace-GGN

The diagonal Laplace-GGN requires backpropagation of $C \times C$ matrices $\Lambda(\mathbf{y}; \mathbf{f})$ (Dangel et al., 2019) and is therefore not as fast as the diagonal EF. The determinant computation, however, is only $\mathcal{O}(P)$. Once the diagonal GGN is obtained, hyperparameter updates are as cheap as in the Kronecker-factored case in $\mathcal{O}(P)$ including updates to the determinant. Empirically, the diagonal Laplace-GGN is not significantly faster than the Kronecker-factored Laplace but it makes a different approximation and therefore might under some circumstances work better (see App. C.4).

B.5. Diagonal Laplace-EF

The diagonal Laplace-EF is cheaper and simpler to compute than the diagonal Laplace-GGN while maintaining the same hyperparameter update complexity of $\mathcal{O}(P)$. To compute the EF while passing through the training data, we only need to compute individual gradients, square them element-wise, and sum them up. Hence, this is as cheap as a pass through the training data for neural network parameters (roughly $\mathcal{O}(NP)$). One hyperparameter update is then $\mathcal{O}(P)$.

C. Experimental details and additional results

C.1. Illustrative examples

We complement the results of Sec. 4.1 with Bayesian predictives obtained after running our online algorithm.

Bayesian regression predictive. For a Gaussian likelihood, the Bayesian predictive (cf. Eq. 11) has a closed-form and we do not need samples (Foong et al., 2019; Khan et al., 2019; Immer et al., 2021). We additionally show the Bayesian predictive and its decomposition in epistemic and aleatoric uncertainty for the illustrative regression example in Fig. 3. The aleatoric, irreducible, uncertainty is the noise in the data. The epistemic uncertainty is model-dependent and quantifies how certain a model is about its prediction. In the regression example, the aleatoric uncertainty is the observation noise σ^2 that we learn online and the epistemic uncertainty is the model uncertainty $\text{Var}[\mathbf{f}]$ which we optimize implicitly via the prior. The variance of the posterior predictive is then $\text{Var}[\mathbf{f}] + \sigma^2$ and the standard deviation is not additive. In Fig. C.1a, we split

Scalable Marginal Likelihood Estimation for Model Selection in Deep Learning

Dataset	MAP	cross-validation		MargLik optimization					
		VI	Laplace	GGN-Bayes	GGN-MAP	EF-Bayes	EF-MAP	KFAC-Bayes	KFAC-MAP
boston	2.71±0.10	2.58±0.03	2.57±0.05	2.68±0.12	2.69±0.13	2.60±0.09	2.62±0.12	2.70±0.08	2.70±0.09
concrete	3.17±0.04	3.17±0.01	3.05±0.04	3.06±0.05	3.06±0.05	3.07±0.04	3.07±0.04	3.13±0.06	3.13±0.06
energy	1.02±0.05	1.42±0.01	0.82±0.03	0.54±0.11	0.55±0.11	0.78±0.13	0.73±0.15	0.54±0.02	0.53±0.02
kin8nm	-1.09±0.01	-0.87±0.00	-1.23±0.01	-1.14±0.01	-1.14±0.01	-1.13±0.01	-1.14±0.01	-1.13±0.01	-1.13±0.01
naval	-5.75±0.05	-3.82±0.02	-6.40±0.06	-6.61±0.03	-6.93±0.03	-6.21±0.05	-6.92±0.04	-6.32±0.05	-6.88±0.05
power	2.82±0.01	2.86±0.01	2.83±0.01	2.78±0.02	2.78±0.02	2.78±0.01	2.78±0.01	2.78±0.02	2.78±0.02
wine	0.98±0.02	0.96±0.01	0.97±0.02	0.94±0.02	0.93±0.02	0.94±0.01	0.93±0.02	0.94±0.02	0.94±0.02
yacht	2.30±0.02	1.67±0.01	1.01±0.05	3.51±0.62	5.89±1.25	1.29±0.17	2.43±0.61	1.48±0.07	1.48±0.07

Table C2: Additional performance of the Bayesian posterior predictive on the UCI regression benchmark complementing Table 1. The posterior predictive does not significantly improve the predictive except on the yacht data set which is very small and might require better uncertainty quantification.

Dataset	GGN-Bayes	GGN-MAP	diag-GGN-Bayes	diag-GGN-MAP	diag-EF-Bayes	diag-EF-MAP
boston	2.68±0.12	2.69±0.13	2.84±0.05	2.84±0.05	2.90±0.03	2.89±0.03
concrete	3.06±0.05	3.06±0.05	3.13±0.04	3.13±0.04	3.11±0.02	3.11±0.02
energy	0.54±0.11	0.55±0.11	0.70±0.03	0.69±0.03	0.88±0.05	0.85±0.05
kin8nm	-1.14±0.01	-1.14±0.01	-1.14±0.01	-1.13±0.01	-1.13±0.01	-1.13±0.01
naval	-6.61±0.03	-6.93±0.03	-6.17±0.05	-6.91±0.08	-5.83±0.06	-6.95±0.04
power	2.78±0.02	2.78±0.02	2.79±0.02	2.79±0.02	2.79±0.01	2.79±0.01
wine	0.94±0.02	0.93±0.02	0.96±0.01	0.95±0.02	0.98±0.01	0.96±0.02
yacht	3.51±0.62	5.89±1.25	2.91±0.04	2.90±0.04	3.16±0.02	3.15±0.02

Table C3: Performance on UCI regression tasks of the diagonal EF and GGN online marginal likelihood optimization method compared to the full GGN which performs best. The diagonal approximation slightly decreases the performance but is not significantly worse. In comparison to a cross-validated MAP, the cheap diagonal approximations still perform quite well (cf. first column in Table C2).

up the total predictive variance approximately so that the observation noise σ is depicted exactly and the model uncertainty is just the remaining standard deviation.

Bayesian classification predictive. Fig. C.1b depicts the Bayesian predictives corresponding to the schematic figure Fig. 3. We use $S = 1000$ samples to estimate the posterior predictive in Eq. 11. The samples are on the output of the network and are therefore cheap (Immer et al., 2021). The Bayesian predictive of the model with a better marginal likelihood has increasing uncertainty away from the data as often desired (Foong et al., 2019). The parameters found by our online algorithm give rise to a Bayesian predictive without further tuning of parameters after training which is required when using the Laplace approximation (Ritter et al., 2018; Kristiadi et al., 2020). Alternatively, one can run a grid-search to find suitable parameters (Khan et al., 2019; Immer et al., 2021). Our algorithm is more principled than changing the prior after training and significantly more efficient than a grid-search.

Regression grid search. In Fig. 4, we compared a grid-search over a single prior parameter with the online optimization algorithm and show it converges to the optimum marginal likelihood with different initializations. Here, we additionally show in Fig. C.2 that the best marginal likelihood also corresponds to the best negative log likelihood (nll) on the held-out test set. The online optimization algorithm reliably finds the optimum without access to the test data.

C.2. UCI regression

We complement the results presented in Sec. 4.2 and in Table 1 with the performance of the optional Bayesian posterior predictive and of the diagonal determinant approximations. We always report the performance of the posterior predictive using the posterior of the same structure as the determinant approximation during marginal likelihood optimization, e.g., if we use the full EF during optimization, we use the Laplace-EF posterior and make predictions with it using Eq. 11. In Table C2, we report the performance of the additional posterior predictive for the full GGN, EF, and KFAC determinant computations and their corresponding posterior predictive. The MAP predictive overall seems to perform better except on the small yacht data set. Table C3 further shows the performance when using the diagonal GGN or EF approximations.

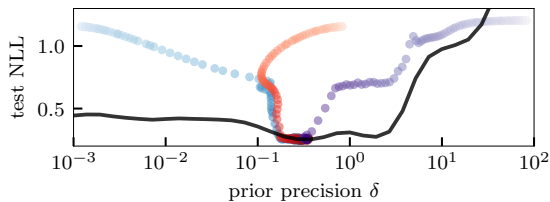


Figure C.2: Test negative log likelihood versus prior precision δ corresponding to Fig. 4. The proposed method reliably converges to the optimal predictive performance.

Scalable Marginal Likelihood Estimation for Model Selection in Deep Learning

Dataset	MAP	cross-validation		GGN-Bayes	GGN-MAP	MargLik optimization		KFAC-Bayes	KFAC-MAP
		VI	Laplace			EF-Bayes	EF-MAP		
australian	0.32±0.01	0.32±0.01	0.32±0.01	0.31±0.01	0.31±0.01	0.34±0.01	0.31±0.01	0.32±0.01	0.31±0.01
cancer	0.13±0.03	0.17±0.05	0.10±0.01	0.10±0.01	0.09±0.01	0.25±0.01	0.10±0.02	0.10±0.01	0.09±0.01
ionosphere	0.28±0.02	0.23±0.02	0.28±0.01	0.29±0.02	0.26±0.03	0.42±0.01	0.28±0.04	0.31±0.02	0.29±0.02
glass	0.89±0.03	1.07±0.07	0.88±0.01	0.92±0.02	0.91±0.05	1.37±0.02	1.03±0.10	0.98±0.02	0.98±0.04
vehicle	0.39±0.01	0.37±0.01	0.46±0.00	0.47±0.01	0.41±0.01	0.75±0.01	0.38±0.01	0.49±0.00	0.45±0.01
waveform	0.36±0.00	0.35±0.00	0.37±0.00	0.35±0.01	0.34±0.01	0.43±0.01	0.36±0.02	0.35±0.01	0.34±0.01
digits	0.08±0.00	0.14±0.01	0.26±0.00	0.31±0.01	0.13±0.01	1.81±0.01	0.07±0.01	0.30±0.01	0.16±0.01
satellite	0.23±0.00	0.28±0.00	0.25±0.00	0.25±0.00	0.22±0.01	0.68±0.01	0.24±0.01	0.25±0.00	0.24±0.00

(a) Negative test log likelihood (lower better)

Dataset	MAP	cross-validation		GGN-Bayes	GGN-MAP	MargLik optimization		KFAC-Bayes	KFAC-MAP
		VI	Laplace			EF-Bayes	EF-MAP		
cancer	96.8±0.4	96.4±0.4	97.0±0.3	96.8±0.4	96.9±0.4	96.7±0.5	96.7±0.5	96.7±0.5	96.7±0.5
ionosphere	90.6±0.7	92.6±0.7	90.6±0.6	90.0±1.3	90.0±1.3	90.9±1.2	91.5±1.0	89.1±1.3	88.9±1.4
glass	67.2±1.4	63.4±1.4	65.3±1.4	64.4±2.7	64.1±2.8	65.9±2.7	67.8±2.2	63.7±2.0	64.7±1.9
vehicle	83.2±0.3	81.4±0.4	80.9±0.3	81.7±0.9	82.0±0.9	82.1±0.6	83.2±0.5	80.3±0.8	80.3±0.8
waveform	85.7±0.3	85.6±0.3	85.7±0.3	85.9±0.6	85.9±0.5	84.7±0.8	84.3±0.8	86.0±0.5	85.9±0.6
digits	98.1±0.1	97.3±0.1	97.1±0.1	97.3±0.2	97.4±0.2	86.9±0.8	98.1±0.2	97.0±0.4	97.1±0.3
satellite	91.6±0.1	89.9±0.1	91.3±0.1	91.6±0.2	91.6±0.3	91.1±0.4	91.5±0.3	91.0±0.2	91.0±0.2

(b) Test accuracy (higher better)

Dataset	MAP	cross-validation		GGN-Bayes	GGN-MAP	MargLik optimization		KFAC-Bayes	KFAC-MAP
		VI	Laplace			EF-Bayes	EF-MAP		
australian	0.06±0.01	0.06±0.00	0.07±0.01	0.07±0.01	0.05±0.01	0.09±0.01	0.06±0.00	0.06±0.01	0.06±0.01
cancer	0.03±0.00	0.03±0.00	0.03±0.00	0.03±0.00	0.03±0.00	0.18±0.01	0.03±0.00	0.03±0.00	0.03±0.00
ionosphere	0.08±0.00	0.07±0.00	0.11±0.00	0.10±0.01	0.08±0.01	0.22±0.01	0.06±0.01	0.10±0.01	0.08±0.01
glass	0.17±0.01	0.17±0.01	0.19±0.01	0.18±0.02	0.17±0.01	0.36±0.02	0.18±0.02	0.19±0.02	0.18±0.01
vehicle	0.06±0.00	0.07±0.00	0.10±0.00	0.12±0.01	0.07±0.01	0.30±0.01	0.06±0.01	0.12±0.01	0.08±0.01
waveform	0.05±0.00	0.04±0.00	0.06±0.00	0.07±0.00	0.05±0.01	0.12±0.01	0.05±0.00	0.07±0.00	0.05±0.00
digits	0.01±0.00	0.03±0.00	0.17±0.00	0.20±0.00	0.06±0.00	0.70±0.01	0.01±0.00	0.19±0.00	0.08±0.00
satellite	0.02±0.00	0.02±0.00	0.04±0.00	0.05±0.00	0.02±0.00	0.36±0.00	0.02±0.00	0.05±0.00	0.03±0.00

(c) Test expected calibration error (lower better)

Dataset	GGN-Bayes	GGN-MAP	diag-GGN-Bayes	diag-GGN-MAP	diag-EF-Bayes	diag-EF-MAP
australian	0.31±0.01	0.31±0.01	0.35±0.01	0.33±0.01	0.34±0.01	0.32±0.01
cancer	0.10±0.01	0.09±0.01	0.12±0.01	0.09±0.01	0.16±0.01	0.09±0.01
ionosphere	0.29±0.02	0.26±0.03	0.38±0.01	0.35±0.01	0.37±0.01	0.31±0.02
glass	0.92±0.02	0.91±0.05	1.09±0.01	1.06±0.02	1.05±0.02	0.99±0.03
vehicle	0.47±0.01	0.41±0.01	0.75±0.01	0.68±0.01	0.71±0.01	0.59±0.01
waveform	0.35±0.01	0.34±0.01	0.41±0.01	0.38±0.01	0.40±0.01	0.37±0.01
digits	0.31±0.01	0.13±0.01	0.43±0.00	0.23±0.01	0.97±0.02	0.09±0.01
satellite	0.25±0.00	0.22±0.01	0.34±0.00	0.30±0.00	0.35±0.00	0.29±0.00

(d) Negative test log likelihood (lower better) of diag-GGN and diag-EF compared to full GGN.

Table C4: Performance of the proposed online marginal likelihood optimization method compared to cross-validation on UCI classification benchmark using a ReLU network with 50 units and one hidden layer. The marginal likelihood optimization leads to comparable performance as cross-validation and the MAP typically performs better than Laplace or VI. The full EF approximation performs best, followed by the GGN and KFAC approximations. Table C4d shows that the diagonal approximations perform worse, especially when combined with a Bayesian predictive, but are still on a similar level as VI with cross-validation. Results within one standard error are in bold.

C.3. UCI classification

We present additional results on small-scale UCI classification data sets in Table C4. The setup is identical to that in the regression case but we use a different train/validation/test split of 70%/15%/15% here. We use the same architecture as in the regression case, a single hidden layer with 50 units and ReLU activation and train for 10,000 iterations until convergence with all methods. For the grid-search we try 10 different scalar prior precision values δ and select the best parameter on the validation set before re-training. We compare the resulting cross-validated performance to our online algorithm with full GGN, EF, and KFAC approximation to the determinant in Table C4. All methods perform quite well in this benchmark and there are no obvious differences in the negative log likelihood (nll) in Table C4a. However, the cross-validated MAP and full EF-MAP perform better than most other methods in terms of accuracy and expected calibration error.

C.4. Image Classification: online algorithm compared to cross-validation

We provide additional details and the following additional results on the image classification experiments presented in Sec. 4.3: the standard errors for Table 2, the performance of the diagonal GGN, and a comparison of different ResNet depths on CIFAR-10.

Architectures. We compare a fully-connected, convolutional, and residual neural network in our experiments. The fully-connected network has four hidden layers with decreasing hidden layer sizes 1024, 512, 256, 128. For MNIST and FMNIST, this architecture has $P = 1,494,154$ parameters. As a standard convolutional neural network, we use a network of three convolutional layers followed by three fully-connected layers. This network is used in standard benchmarks, for example the suite by Schneider et al. (2018). On MNIST and FMNIST, this architecture has $P = 892,010$ parameters and on CIFAR-10 it has $P = 895,210$ parameters due to the additional color channels in the input. On CIFAR-10, we additionally use a ResNet-20 architecture with $P = 268,393$ parameters using the Fixup parameterization (Zhang et al., 2019b)⁴. We find that increasing the depth of the ResNet up to a ResNet-110 did not improve the performance and marginal likelihood significantly as we show below in Table C8. There, we additionally use ResNets with depths 32, 44, 56, 110 which have $P = 461,959$, $P = 655,525$, $P = 849,091$, and $P = 1,720,138$ parameters, respectively.

Diagonal GGN and standard errors. Table C5 contains the additional standard errors that were left out in the main text in Table 2 due to space constraints. In Table C6, we compare the performance of our method using the diagonal EF and the diagonal GGN. The latter has been left out in the image classification benchmark in the main text. The table shows that the EF works consistently better. Note that the EF is also significantly cheaper to compute and easier to implement than the other methods.

Dataset	Model	cross-validation		MargLik optimization			diagonal EF		MargLik
		accuracy	logLik	accuracy	KFAC logLik	MargLik	accuracy	logLik	
MNIST	MLP	98.22±0.13	-0.061±0.004	98.38±0.04	-0.053±0.002	-0.158±0.001	97.05±0.09	-0.095±0.002	-0.553±0.021
	CNN	99.40±0.03	-0.017±0.001	9.46±0.01	-0.016±0.001	-0.064±0.000	9.45±0.03	-0.019±0.001	-0.134±0.001
FMNIST	MLP	88.09±0.10	-0.347±0.005	89.83±0.14	-0.305±0.006	-0.468±0.002	85.72±0.09	-0.400±0.003	-0.756±0.005
	CNN	91.39±0.11	-0.258±0.004	92.06±0.10	-0.233±0.004	-0.401±0.001	91.69±0.15	-0.233±0.003	-0.570±0.003
CIFAR10	CNN	77.41±0.06	-0.680±0.004	80.46±0.10	-0.644±0.010	-0.967±0.003	80.17±0.29	-0.600±0.010	-1.359±0.010
	ResNet	83.73±0.28	-1.060±0.022	86.11±0.39	-0.595±0.017	-0.717±0.003	85.82±0.13	-0.464±0.007	-0.876±0.012

Table C5: Standard errors for Table 2 in the main text. Best performances within one standard error per dataset in bold.

Dataset	Model	accuracy	diagonal EF		diagonal GGN		
			logLik	MargLik	accuracy	logLik	MargLik
MNIST	MLP	97.05±0.09	-0.095±0.002	-0.553±0.021	96.86±0.04	-0.102±0.002	-0.617±0.014
	CNN	99.45±0.03	-0.019±0.001	-0.134±0.001	99.35±0.02	-0.021±0.001	-0.193±0.001
FMNIST	MLP	85.72±0.09	-0.400±0.003	-0.756±0.005	85.36±0.21	-0.410±0.006	-0.844±0.016
	CNN	91.69±0.15	-0.233±0.003	-0.570±0.003	91.69±0.09	-0.237±0.003	-0.641±0.002
CIFAR10	CNN	80.17±0.29	-0.600±0.010	-1.359±0.010	79.98±0.46	-0.587±0.013	-1.568±0.010

Table C6: Comparison of diagonal GGN and EF on the image classification benchmark. The diagonal EF as presented in Table 2 performs slightly better on all datasets and is cheaper to compute.

KFAC results for CIFAR-10 with data augmentation. We presented the performance of the marginal likelihood optimization using diagonal EF on CIFAR-10 with and without data augmentation (DA) in Fig. 5. In Table C7, we provide the results in terms of average performance over five random seeds and the performance of the KFAC GGN variant. On this benchmark, we see that the cheaper diagonal EF performs typically slightly better while being more efficient than the KFAC variant.

Deeper ResNets. In the main text, we only presented results for a ResNet-20. That is because we found that a depth over 20 for CIFAR-10 did not improve the marginal likelihood or performance noticeably. Here, we briefly present the corresponding results with and without data augmentation. Interestingly, the optimized marginal likelihood is largely unaffected by the almost 10-fold increase of parameters. In Table C8, we show the performances, marginal likelihoods, and

⁴Their implementation is publicly available with the corresponding standard settings on CIFAR-10: <https://github.com/hongyi-zhang/Fixup>

Scalable Marginal Likelihood Estimation for Model Selection in Deep Learning

Dataset	Method	accuracy	logLik	ECE	OOD-AUC
CIFAR-10	baseline	83.73±0.28	-1.06±0.02	0.127±0.002	0.814±0.007
CIFAR-10	MargLik diag EF	85.82±0.13	-0.46±0.01	0.048±0.002	0.901±0.004
CIFAR-10	MargLik KFAC GGN	86.11±0.39	-0.60±0.02	0.085±0.003	0.882±0.008
CIFAR-10 + DA	baseline	91.38±0.15	-0.58±0.01	0.069±0.001	0.897±0.003
CIFAR-10 + DA	MargLik diag EF	91.18±0.20	-0.38±0.02	0.054±0.003	0.900±0.003
CIFAR-10 + DA	MargLik KFAC GGN	91.26±0.12	-0.54±0.02	0.068±0.001	0.896±0.006

Table C7: Results displayed in Fig. 5 with additional results for the marginal likelihood training based on KFAC GGN.

parameters with standard errors over five initializations. Without data augmentation, the smaller models are preferred. With data augmentation, the medium-sized models fare best in terms of marginal likelihood.

Model	P	no DA			with DA		
		accuracy	logLik	MargLik	accuracy	logLik	MargLik
ResNet-20	268,393	85.82±0.13	-0.46±0.01	-0.876±0.012	91.18±0.20	-0.375±0.020	-0.633±0.002
ResNet-32	461,959	85.66±0.29	-0.46±0.01	-0.898±0.025	91.63±0.22	-0.355±0.017	-0.623±0.008
ResNet-44	655,525	85.63±0.24	-0.45±0.01	-0.904±0.014	91.78±0.11	-0.336±0.007	-0.622±0.009
ResNet-56	849,091	85.82±0.17	-0.44±0.01	-0.932±0.010	91.62±0.15	-0.344±0.012	-0.625±0.013
ResNet-110	1,720,138	86.11±0.24	-0.44±0.01	-0.937±0.009	91.85±0.13	-0.323±0.009	-0.638±0.009

Table C8: ResNets of various depths trained on CIFAR-10 and their sizes, performances, and marginal likelihoods with and without data augmentation (DA). Without data augmentation, the smallest model achieves the highest marginal likelihood and the performances of all models are very close to each other. With data augmentation, the marginal likelihoods overlap in terms of their standard errors but a ResNet-44 seems best. Notably, the increase of the number of parameters P does not significantly impact the marginal likelihood.

C.5. Image Classification: architecture selection using the marginal likelihood

We presented results on architecture selection using MargLik in Sec. 4.3, Fig. 2, and Fig. 7. Fig. 7 is the upper right of Fig. 2 and only shows the ResNets colored by width and depth. Here, we describe details on the experimental setup and architectures, and list more detailed results.

Model training. All models were trained using Alg. 1 for 250 epochs, frequency $F = 5$, $K = 100$ hyperparameter updates with learning rate $\gamma = 1$, and no burnin $B = 0$. We use the ResNet learning rate decay as explained in Sec. 4 for all models and train with SGD with initial learning rate of 0.01 and a batch-size of 128.

Architectures. On FMNIST we compare MLPs and CNNs, and on CIFAR we compare CNNs and ResNets. For the MLPs, we use 3 different widths 50, 200, 800 and depth from 1 to 5. The CNNs consist of up to 5 blocks of 3×3 convolutions, followed by a ReLU operation, and MaxPooling, except in the first layer. Instead of BatchNorm, we use the fixup parameterization (Zhang et al., 2019b) after every convolutional layer. For the widths, we consider widths, i.e., number of channels, from 2 to 32 in the first convolution. Each following convolution uses $2 \times$ more channels such that after three convolutions the number of channels is $2^3 = 8$ times higher. The last layer is a fully-connected layer to the class logits. We use ResNets of depths from 8 to 32 on CIFAR-10 and from 20 to 101 on CIFAR-100. On CIFAR-10, more depth does not further increase or change the marginal likelihood, see Table C8. For the width, we vary the number of channels in the first convolutional layer. For CIFAR-10, we consider widths from 16 to 48 and on CIFAR-100 from 32 to 64. All the architectures on the corresponding data sets are listed with the marginal likelihood, accuracy, number of parameters, width, and depth in Table C11 (FMNIST), Table C9 (CIFAR-10), and Table C10 (CIFAR-100).

Additional figures. The markers in the scatter plots of architectures are colored and scaled by the number of parameters in Fig. 2. Here, we additionally show a coloring and scaling by width and depth in Fig. C.3 and Fig. C.4, respectively. Fig. C.3 shows that width tends to increase marginal likelihood and test accuracy on CIFAR. This is in line with improved ResNet architectures that proposed increasing the width (Zagoruyko & Komodakis, 2016). On FMNIST, the comparison between MLPs and CNNs is not meaningful in terms of width since width on CNNs determines the number of channels instead of hidden units. However, we can see that less wide MLPs achieve a better marginal likelihood and test accuracy. Fig. C.4 shows that increased depth does increase the marginal likelihood but saturates much earlier than width. For example, ResNets, which are deeper, are generally preferred over CNNs on CIFAR but the best models are not the deepest ResNets, see also Table C9 and Table C10. On FMNIST, we see in Fig. C.4 how the depth tends to decrease marginal likelihood and test accuracy of MLPs. Contrary to that, CNNs profit significantly from increasing the depth.

C.6. Robustness to algorithm hyperparameters

Alg. 1 has four different hyperparameters that need to be set. K determines how many gradient steps we take on the marginal likelihood objective. F determines how frequently we compute the marginal likelihood and optimize it with respect to hyperparameters. B determines for how many epochs we do not optimize the marginal likelihood, similar to a burn-in period in MCMC algorithms. On CIFAR-10, we conduct an ablation experiment running over a grid of these hyperparameters. Below, we make recommendations on how to apply our algorithm based on the outcomes of this experiment.

Step size γ . The step size γ only needs to be set to ensure the marginal likelihood objective does not diverge. γ does not affect the runtime but only convergence behavior. We find that using ADAM with default learning rate of $\gamma = 0.001$ works well but we can increase the learning rate without divergence to $\gamma = 1$ which ultimately decreases the number of steps K we need to take every F -th epoch to observe convergence. To set γ , a practitioner only needs to monitor the marginal likelihood or the parameters and avoid divergence or oscillation.

Frequency and number of steps. Number of steps K , frequency F , and burn-in steps B can be used to reduce the runtime by avoiding to compute the Laplace approximation too often. B is only a mechanism to reduce the runtime in the early training regime where the parameters of the network θ are very noisy. If affordable, $B = 0$ is optimal for performance but we find that $B = 50$ works equivalently well. In many cases, convergence of the neural network training can even be improved by adjusting hyperparameters early. K and F determine how many hyperparameter steps we take and how many Laplace approximations need to be computed, respectively. Computing the Laplace approximation is expensive while hyperparameter steps are *amortized*, i.e., once we computed the Laplace approximation it is cheap to do many gradient steps K (cf. App. B). It is therefore ideal for performance to have $F = 1$ and compute the Laplace approximation after every epoch and have a large number of steps K . In practice, however, we find that F between 5 and 10 is sufficient and does not decrease performance. Further, $K \geq 100$ also appears to suffice for convergence with no gain using $K = 1000$.

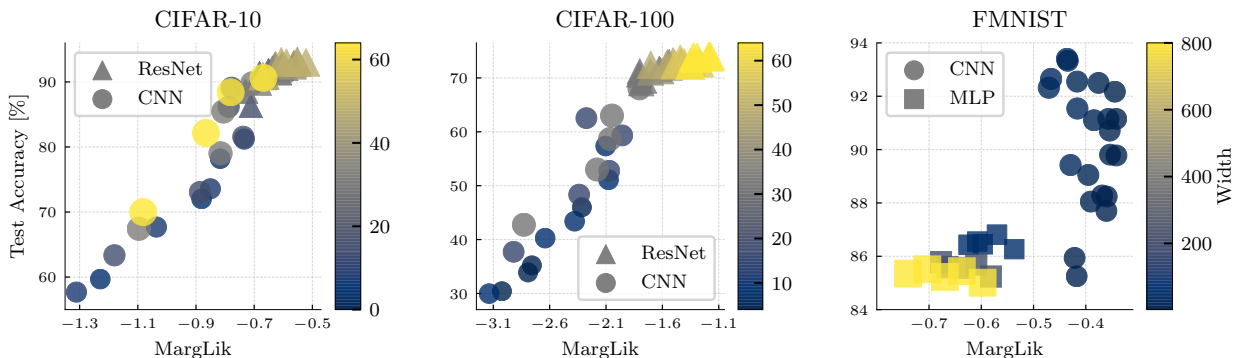


Figure C.3: Figure corresponds to Fig. 2 but shows markers colored and scaled by width.

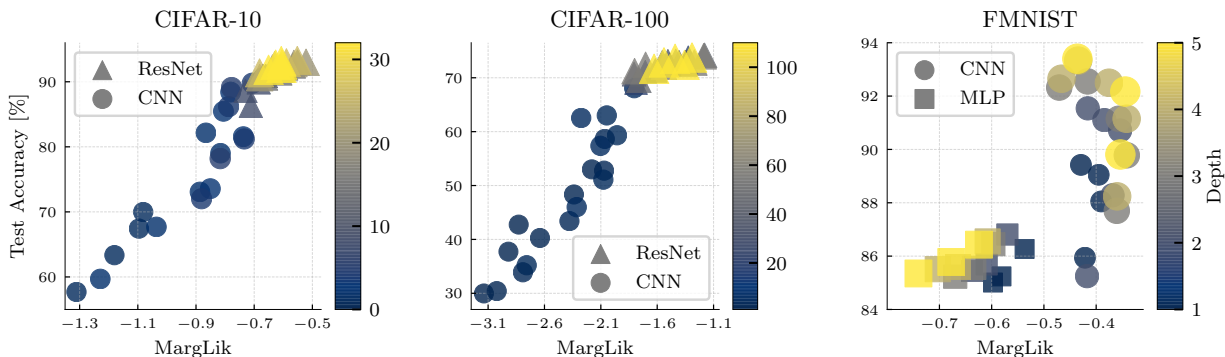


Figure C.4: Figure corresponds to Fig. 2 but shows markers colored and scaled by depth.

Scalable Marginal Likelihood Estimation for Model Selection in Deep Learning

accuracy	MargLik	width	depth	# params	model
85.01	-0.598	800	1	636,034	MLP
85.23	-0.670	800	3	1,917,650	MLP
85.24	-0.581	200	1	159,034	MLP
85.25	-0.417	2	2	566	CNN
85.35	-0.740	800	5	3,199,266	MLP
85.44	-0.637	800	2	1,276,842	MLP
85.51	-0.703	800	4	2,558,458	MLP
85.56	-0.633	200	3	239,450	MLP
85.59	-0.664	200	4	279,658	MLP
85.69	-0.610	200	2	199,242	MLP
85.78	-0.677	200	5	319,866	MLP
85.94	-0.421	4	1	748	CNN
86.27	-0.537	50	1	39,784	MLP
86.43	-0.624	50	5	50,016	MLP
86.45	-0.597	50	3	44,900	MLP
86.55	-0.608	50	4	47,458	MLP
86.81	-0.570	50	2	42,342	MLP
87.70	-0.361	2	3	864	CNN
88.05	-0.390	8	1	1428	CNN
88.24	-0.360	2	4	2074	CNN
88.28	-0.369	4	2	1166	CNN
89.05	-0.395	16	1	2788	CNN
89.42	-0.429	32	1	5508	CNN
89.78	-0.341	4	3	2296	CNN
89.81	-0.354	2	5	6756	CNN
90.71	-0.354	8	2	2798	CNN
91.10	-0.384	16	2	7790	CNN
91.15	-0.342	4	4	6978	CNN
91.15	-0.357	8	3	7320	CNN
91.54	-0.416	32	2	24,686	CNN
92.17	-0.344	4	5	25,516	CNN
92.32	-0.471	32	3	97,944	CNN
92.50	-0.376	8	4	25,858	CNN
92.55	-0.417	16	3	26,008	CNN
92.65	-0.466	32	4	393,154	CNN
93.33	-0.434	16	4	99,906	CNN
93.40	-0.436	32	5	1,573,356	CNN

Table C11: FMNIST architectures

accuracy	MargLik	width	depth	# params	model	accuracy	MargLik	width	depth	# params	model
57.69	-1.311	8	1	1572	CNN	23.54	-3.435	4	1	6670	CNN
59.69	-1.229	4	2	1238	CNN	29.97	-3.137	8	1	13,182	CNN
63.35	-1.180	16	1	3076	CNN	30.41	-3.023	4	2	7808	CNN
67.43	-1.096	32	1	6084	CNN	33.90	-2.791	4	3	8218	CNN
67.69	-1.036	8	2	2942	CNN	35.21	-2.758	4	4	12,900	CNN
69.98	-1.081	64	1	12,100	CNN	37.73	-2.920	16	1	26,206	CNN
72.02	-0.881	4	4	7050	CNN	40.27	-2.640	8	2	15,992	CNN
73.07	-0.886	16	2	8078	CNN	42.75	-2.829	32	1	52,254	CNN
73.57	-0.851	8	3	7464	CNN	43.40	-2.379	8	3	19,074	CNN
78.20	-0.817	4	5	25,588	CNN	45.99	-2.314	4	5	31,438	CNN
79.02	-0.816	32	2	25,262	CNN	48.34	-2.339	16	2	34,088	CNN
81.21	-0.734	8	4	26,002	CNN	51.09	-2.078	8	4	37,612	CNN
81.56	-0.737	16	3	26,296	CNN	52.76	-2.071	16	3	49,426	CNN
82.15	-0.866	64	2	87,278	CNN	53.00	-2.180	32	2	77,192	CNN
85.46	-0.806	32	3	98,520	CNN	57.36	-2.103	8	5	111,510	CNN
86.18	-0.788	16	4	100,194	CNN	58.65	-2.065	32	3	144,690	CNN
86.30	-0.712	16	8	75,129	ResNet	59.33	-1.956	16	4	123,324	CNN
88.41	-0.781	64	3	381,208	CNN	62.54	-2.274	16	5	418,534	CNN
88.58	-0.730	24	8	167,825	ResNet	63.01	-2.047	32	4	439,900	CNN
89.10	-0.778	16	5	395,404	CNN	68.07	-1.804	32	5	1,620,102	CNN
89.78	-0.706	32	4	393,730	CNN	69.01	-1.788	32	20	1,083,601	ResNet
89.90	-0.685	32	8	297,385	ResNet	69.50	-1.763	32	44	2,632,813	ResNet
90.62	-0.662	16	14	172,128	ResNet	70.65	-1.805	32	32	1,858,207	ResNet
90.62	-0.668	64	4	1,561,410	CNN	71.11	-1.706	40	20	1,688,361	ResNet
90.63	-0.681	16	20	269,127	ResNet	71.22	-1.801	32	56	3,407,419	ResNet
90.89	-0.660	40	8	463,809	ResNet	71.35	-1.616	40	32	2,898,423	ResNet
90.90	-0.670	48	8	667,097	ResNet	71.66	-1.627	32	110	6,893,146	ResNet
91.37	-0.682	16	26	366,126	ResNet	72.02	-1.540	40	56	5,318,547	ResNet
91.40	-0.613	24	14	385,784	ResNet	72.36	-1.562	48	20	2,426,753	ResNet
91.83	-0.651	16	32	463,125	ResNet	72.38	-1.358	48	110	15,493,898	ResNet
91.97	-0.613	32	20	1,071,991	ResNet	72.40	-1.703	48	56	7,653,611	ResNet
92.09	-0.610	24	26	821,702	ResNet	72.45	-1.487	56	20	3,298,777	ResNet
92.11	-0.637	24	20	603,743	ResNet	72.47	-1.351	64	32	7,401,471	ResNet
92.12	-0.606	24	32	1,039,661	ResNet	72.78	-1.554	40	44	4,108,485	ResNet
92.17	-0.593	32	14	684,688	ResNet	72.78	-1.407	56	44	8,041,333	ResNet
92.47	-0.567	40	14	1,068,840	ResNet	72.82	-1.271	56	56	10,412,611	ResNet
92.50	-0.630	32	26	1,459,294	ResNet	72.85	-1.540	40	110	10,763,826	ResNet
92.62	-0.626	40	32	2,883,933	ResNet	72.90	-1.344	56	32	5,670,055	ResNet
92.66	-0.604	32	32	1,846,597	ResNet	73.02	-1.436	48	44	5,911,325	ResNet
92.81	-0.564	40	20	1,673,871	ResNet	73.05	-1.505	48	32	4,169,039	ResNet
92.93	-0.589	48	26	3,280,526	ResNet	73.51	-1.441	56	110	21,083,362	ResNet
92.98	-0.551	48	14	1,538,240	ResNet	73.75	-1.291	64	110	27,532,218	ResNet
92.99	-0.522	48	20	2,409,383	ResNet	73.82	-1.325	64	20	4,304,433	ResNet
93.16	-0.607	48	32	4,151,669	ResNet	73.98	-1.188	64	56	13,595,547	ResNet
93.29	-0.552	40	26	2,278,902	ResNet	74.16	-1.180	64	44	10,498,509	ResNet

Table C9: CIFAR-10 architectures

Table C10: CIFAR-100 architectures